View metadata, citation and similar papers at core.ac.uk

brought to you by CORE

provided by NASA Technical Reports Server

111-27
110302
p-40

NASA Technical Memorandum 106838

Driving Force Analysis in an Infinite Anisotropic Plate With Multiple Crack Interactions

Wieslaw K. Binienda
The University of Akron
Akron, Ohio

and

Steven M. Arnold
Lewis Research Center
Cleveland, Ohio

January 1995

National Aeronautics and Space Administration

(NASA-TM-106838) DRIVING FORCE ANALYSIS IN AN INFINITE ANISOTROPIC PLATE WITH MULTIPLE CRACK INTERACTIONS (NASA. Lewis Research Center) 40 p

N95-19782

Unclas

G3/24 0040302

Driving Force Analysis in an Infinite Anisotropic Plate With Multiple Crack Interactions

Wieslaw K. Binienda
Department of Civil Engineering
The University of Akron
Akron, OH 44325-3905

Steven M. Arnold
NASA Lewis Research Center
Cleveland, OH 44135

Abstract

The methodology and a rigorous solution formulation are presented for stress intensity factors (SIF's, k) and total strain energy release rates (SERR, G_T) of a multicracked plate, that has fully interacting cracks and is subjected to a far-field arbitrary stress state. The fundamental perturbation problem is derived, and the steps needed to formulate the system of singular integral equations whose solution gives rise to the evaluation of the SIF's are identified. Parametric studies are conducted for two, three and four crack problems. The sensitivity and characteristics of the model is demonstrated.

1 Nomenclature

α	– inclination angle between inner tips of two parallel cracks
β_{lr}, β_{mz}	– direction cosines between two local coordinate systems
ϵ_{jl}	– strain tensor
μ_k	– four roots of the characteristic equation
φ_j	– angle defining orientation of local coordinate system
σ^o_{jl}, $_p(\sigma^T_{jl})$	– far-field and total stress field, respectively
$\sigma^o_{XX}, \sigma^o_{YY}, \sigma^o_{XY}$	– components of stress in global coordinate system
σ^p_{jl}	– stress from the perturbation problem in p^{th} local frame
$\widehat{\sigma}^j_{jl}$	– transformed j^{th} crack stressed to the p^{th} local frame
ξ, τ	– normalized real variables
$\Phi(s,y)$	– Fourier transform of the stress function with respect to x
Ω	– angle between $L-T$ and $X-Y$ coordinate systems

a, b, c, d	–	roots of the characteristic equation (real numbers)
a_j	–	half crack length
$b_{11,12,22,16,26,66}$	–	compliant matrix coefficient in $x_j - y_j$ frame
$f_{\eta j}$	–	auxiliary functions
k_1, k_2	–	mode-I and mode-II stress intensity factors
ker_γ	–	Fredholm kernels
p_j	–	normal traction at crack surface
q_j	–	shear traction at crack surface
$\underline{r_j}$	–	position vector defining the origin of a local coordinate system
r_{jX}, r_{jY}	–	components of the position vector $\underline{r_j}$
s	–	Fourier variable
t	–	real variable along a crack axis
u, v	–	displacement associated with x and y coordinates, respectively
w	–	weight function
(x_j, y_j), (X, Y), (L, T)	–	local, global and material coordinates (L - strong direction)
$[A]$	–	kernel matrix
$B_{11,12,22,66}$	–	compliant matrix coefficient in $L - T$ frame
C_m	–	functions of s in Fourier space (i.e., constants in x, y-real space)
D_j, S_j, R_j, Q_j	–	constants of substitution
D_h, D_v	–	horizontal and vertical distances between crack tips
$E_{LL}, E_{TT}, G_{LT}, \nu_{LT}$	–	material's parameters in $L - T$ frame
$E^{p(1)}_{xy}, E^{p(1)}_{yy}, E^{p(2)}_{xy}, E^{p(2)}_{yy}$	–	modified stiffness parameters
$F_j(x_j, y_j)$	–	Airy stress function
G_T	–	total strain energy release rate
$H_{\eta j}(\tau_p)$	–	discrete auxiliary function
K_{eff}	–	effective stress intensity factor
$\{\mathcal{R}\}$	–	loading vector
$Q_j^{(iso)}, Q_j^{(reg)}$	–	(iso) stands for isotropic singular, (reg) for nonsingular part

2 INTRODUCTION

Consider multiple cracks embedded in an infinite anisotropic plate (Fig. 1(a)). The plate is under a far-field stress denoted by σ^o_{jl}, (in particular σ^o_{XX}, σ^o_{YY}, and σ^o_{XY}, where (X,Y) is the global coordinate system), and the cracks are defined in their local frames (x_j,y_j) (Fig. 1(b)). The origin of each local frame is defined by the position vector $\underline{r_j}$, and the orientation of the local frame with respect to the global frame is defined by the angle φ_j. Each crack is symmetrically situated within its own coordinate system and is $2a_j$ long, as shown in Fig. 1(b).

The general solution formulation can be outlined in four basic steps. The first step is to derive the local stress equations for each crack in its respective local coordinate system. This derivation is achieved by defining the fundamental problem; that is a single crack in an infinite anisotropic plane (Fig. 1(b)). The fundamental problem is then decomposed into two subproblems: the problem of the undamaged plate containing an imaginary crack (Fig. 1(c)), and the perturbation problem (Fig. 1(d)) of a plate with a single crack subjected to the appropriate crack-surface tractions which are found from the solution of the complementary undamaged problem. The analysis of the perturbation

problem leads to singular stresses that govern local crack-tip behavior.

The second step is to formulate the total perturbation stress field for each crack, which includes the interaction of all cracks through the summation of the transformed local stresses of all other cracks. In the third step of the formulation, the total stress equations are normalized. A set of Cauchy-type singular integral equations, expressed in terms of unknown auxiliary functions, is obtained by subjecting the total perturbation stress equations to the crack-surface traction field at each crack location. The fourth and final step of the formulation is to express the stress intensity factors (SIF's, k_1 and k_2) in terms of the discrete auxiliary functions $H_{\eta j}(\tau_p)$ evaluated at each crack tip. These discrete auxiliary functions are obtained by implementing of the Lobatto-Chebyshev collocation technique. Finally, the strain energy release rate (SERR, G_T) is calculated in terms of SIF's.

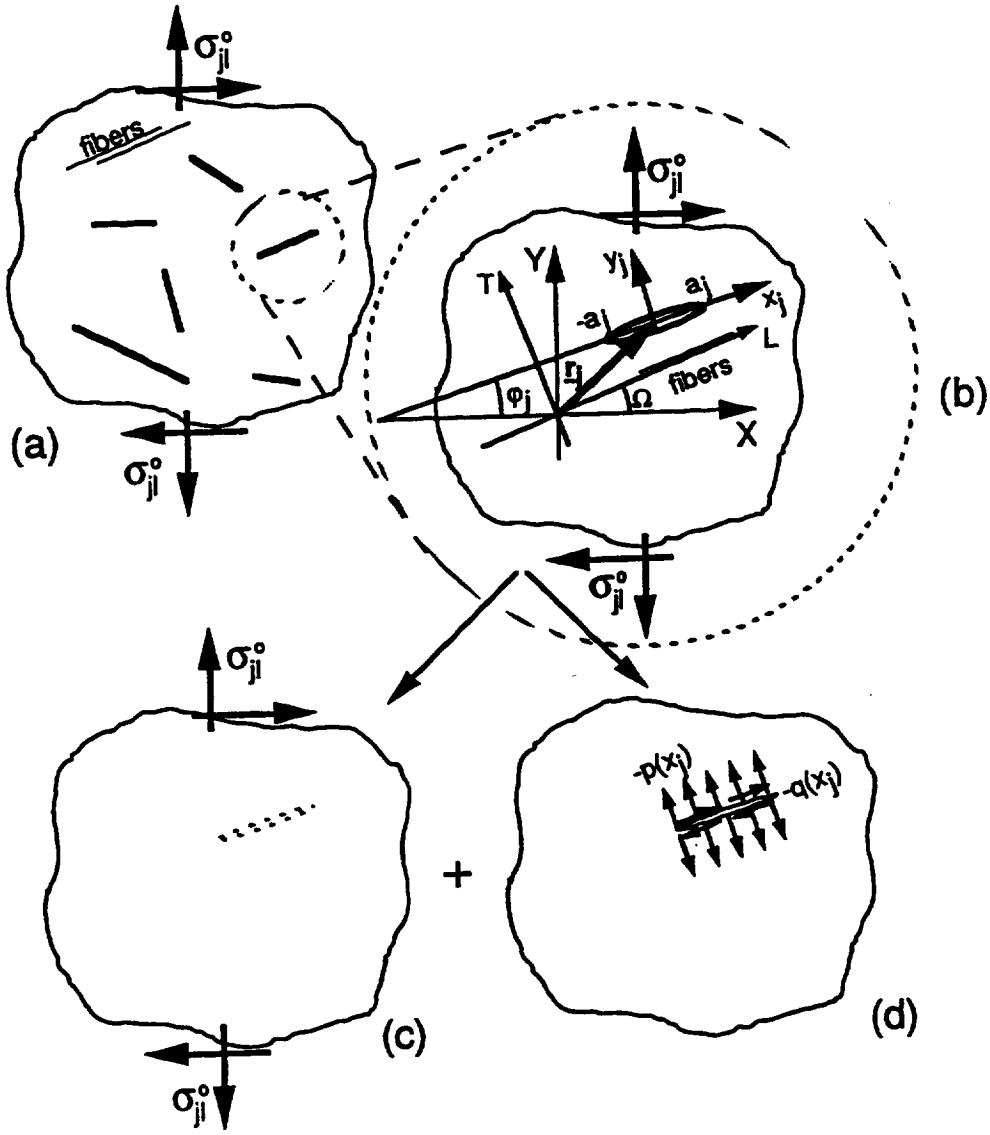

Figure 1: Mulitic racked plate geometry and method of solution. (a) Multicracked plate. (b) Fundamental problem for jth crack. (c) Undamaged plate. (d) Perturbation problem.

3 LOCAL STRESS FORMULATION

Consider the fundamental problem (Fig. 1(b)), which is defined as a single crack in an infinite anisotropic plate; its solution can be obtained by decomposing it into an undamaged problem (Fig. 1(c)) and a perturbation problem (Fig. 1(d)). The essence of this decomposition is that the traction forces applied along the crack surface in the perturbation problem are the opposite of the obtained stress field of the undamaged plate at the particular location of the imaginary crack. As a result, the undamaged plate's traction field can be defined in terms of the normal (p_j) and shear (q_j) stress components along the imaginary crack surface:

$$p_j(x_j) = \sigma_{y_j y_j}(x_j, 0) \tag{1}$$

$$q_j(x_j) = \sigma_{x_j y_j}(x_j, 0) \tag{2}$$

where

$$\sigma_{y_j y_j}(x_j, 0) = \sigma^o_{XX} \sin^2\varphi_j + \sigma^o_{YY} \cos^2\varphi_j - \sigma^o_{XY} \sin\ 2\varphi_j \tag{3}$$

$$\sigma_{x_j y_j}(x_j, 0) = -\frac{\sigma^o_{XX} - \sigma^o_{YY}}{2} \sin\ 2\varphi_j + \sigma^o_{XY} \cos\ 2\varphi_j \tag{4}$$

The mixed boundary conditions for the perturbation part of the fundamental problem (Fig. 1(d)) are expressed in terms of stresses

$$\sigma_{y_j y_j} = -p_j(x_j) \quad \text{and} \quad \sigma_{x_j y_j} = -q_j(x_j) \tag{5}$$

along the crack surface (*i.e.*, $y_j = 0$ *and* $-a_j \le x_j \le a_j$), and in terms of continuity of displacements

$$v^+ = v^- \quad \text{and} \quad u^+ = u^- \tag{6}$$

outside of the crack (*i.e.*, $y_j = 0$ and $|x_j| > a_j$, see Fig. 1(b)). Here the superscript "+" indicates the value of displacement at a point approached from the positive side of the plate, (*i.e.*, $y > 0$), whereas "−" indicates the same point approached from the negative side of the plate (*i.e.*, $y < 0$).

The governing equation for the preceding two-dimensional anisotropic plate problem can be expressed in terms of the Airy stress function $F_j(x_j, y_j)$ as

$$\frac{\partial^4 F}{\partial x^4} + \gamma_1 \frac{\partial^4 F}{\partial x^3 \partial y} + \gamma_2 \frac{\partial^4 F}{\partial x^2 \partial y^2} + \gamma_3 \frac{\partial^4 F}{\partial x \partial y^3} + \gamma_4 \frac{\partial^4 F}{\partial y^4} = 0 \tag{7}$$

where

$$\gamma_1 = -\frac{2b_{26}}{b_{22}}; \qquad \gamma_2 = \frac{2b_{12}+b_{66}}{b_{22}}; \qquad \gamma_3 = -\frac{2b_{16}}{b_{22}}; \quad \text{and} \quad \gamma_4 = \frac{b_{11}}{b_{22}}; \tag{8}$$

Here, for general two-dimensional anisotropy $b_{11}, b_{22}, b_{12}, b_{16}, b_{26}$,and b_{66} are independent.

In this paper, we will be primarily concerned with applications involving unidirectional fiber reinforced composites; these can be idealized at the macrolevel as a pseudo-homogeneous transversely isotropic material. Consequently, the preceding six independent constants now become dependent on the four independent elastic constants, E_{LL}, E_{TT}, G_{LT} and ν_{LT} , where (L,T) is the material coordinate system rotated by the angle Ω with respect to (X,Y), see Fig. 1(b).

Thus,

$$
\begin{aligned}
b_{11} &= B_{11}\cos^4(\Omega-\varphi) + (2B_{12}+B_{66})\sin^2(\Omega-\varphi)\cos^2(\Omega-\varphi) + B_{22}\sin^4(\Omega-\varphi)\\
b_{22} &= B_{22}\cos^4(\Omega-\varphi) + (2B_{12}+B_{66})\sin^2(\Omega-\varphi)\cos^2(\Omega-\varphi) + B_{11}\sin^4(\Omega-\varphi)\\
b_{12} &= B_{12} + (B_{11}+B_{22}-2B_{12}-B_{66})\sin^2(\Omega-\varphi)\cos^2(\Omega-\varphi)\\
b_{66} &= B_{66} + (B_{11}+B_{22}-2B_{12}-B_{66})\sin^2(\Omega-\varphi)\cos^2(\Omega-\varphi)\\
b_{16} &= [B_{22}\sin^2(\Omega-\varphi) - B_{11}\cos^2(\Omega-\varphi) + \tfrac{1}{2}(2B_{12}+B_{66})\cos 2(\Omega-\varphi)]\sin 2(\Omega-\varphi)\\
b_{26} &= [\cos^2(\Omega-\varphi) - \sin^2(\Omega-\varphi) - \tfrac{1}{2}(2B_{12}+B_{66})\cos 2(\Omega-\varphi)]\sin 2(\Omega-\varphi)
\end{aligned}
\tag{9}
$$

where

$$B_{11} = \tfrac{1}{E_{LL}};\quad B_{22} = \tfrac{1}{E_{TT}};\quad B_{12} = \tfrac{-\nu_{LT}}{E_{LL}};\ \text{and}\ \ B_{66} = \tfrac{1}{G_{LT}}$$

Note that this special case of transverse isotropy does not diminish from the generality of the subsequent solution for the general anisotropic case; all that is required to recover the general solution is to experimentally identify the six independent constants used in equation (9).

A rigorous solution for this stress function can be obtained by employing the Fourier transform. Assume the stress function to be expressed as

$$F(x,y) = \frac{1}{2\pi}\int_{-\infty}^{\infty}\sum_{m=1}^{4} C_m e^{\mu_m y s} e^{-isx} ds \tag{10}$$

Then, on substitution into eq. (7) the characteristic equation is obtained. It has four complex roots, which take the following form:

$$
\begin{aligned}
\mu_1 &= a+ib; \quad \mu_2 = c+id;\\
\mu_3 &= -a+ib; \quad \mu_4 = -c+id;
\end{aligned}
\tag{11}
$$

where a and c > 0.

The Airy stress function must also satisfy the physical requirement that the stress function is finite throughout the domain of the plate. Therefore, the following forms of $F_j(x_j, y_j)$, which are automatically bounded at infinity, can be used for the upper half plane (for $y > 0$),

$$F(x,y^+) = \frac{1}{2\pi}\int_{-\infty}^{\infty}\left[C_1 e^{(ibs-a|s|)y} + C_2 e^{(ids-c|s|)y}\right] e^{-isx} ds \tag{12}$$

and for the lower half plane (for $y < 0$),

$$F(x,y^-) = \frac{1}{2\pi}\int_{-\infty}^{\infty}\left[C_3 e^{(ibs+a|s|)y} + C_4 e^{(ids+c|s|)y}\right] e^{-isx} ds \tag{13}$$

Note: Constants C_m for j = 1, 2, 3, and 4 are functions of the Fourier variable s and are determined by using the local stress continuity conditions at the boundaries between the half planes ($y = 0$) and by using the perturbation boundary conditions **subsequent** to the determination of the total stresses at each crack location.

The stresses within the upper and lower half planes are calculated by using the second derivatives of the stress functions [1]. Therefore, the stresses for the upper half plane are

$$\sigma_{xx}^{(+)} = \frac{1}{2\pi}\int_{-\infty}^{\infty}\left[C_1(-a|s|+ibs)^2 e^{(ibs-a|s|)y} + C_2(-c|s|+ids)^2 e^{(ids-c|s|)y}\right] e^{-isx} ds \tag{14}$$

$$\sigma_{yy}^{(+)} = -\frac{1}{2\pi}\int_{-\infty}^{\infty} s^2 \left[C_1 e^{(ibs-a|s|)y} + C_2 e^{(ids-c|s|)y}\right] e^{-isx} ds \tag{15}$$

$$\sigma_{xy}^{(+)} = \frac{1}{2\pi}\int_{-\infty}^{\infty} is \left[C_1 (-a|s| + ibs) e^{(ibs-a|s|)y} + C_2 (-c|s| + ids) e^{(ids-c|s|)y}\right] e^{-isx} ds \tag{16}$$

and for the lower half plane

$$\sigma_{xx}^{(-)} = \frac{1}{2\pi}\int_{-\infty}^{\infty} \left[C_3 (a|s| + ibs)^2 e^{(ibs+a|s|)y} + C_4 (c|s| + ids)^2 e^{(ids+c|s|)y}\right] e^{-isx} ds \tag{17}$$

$$\sigma_{yy}^{(-)} = -\frac{1}{2\pi}\int_{-\infty}^{\infty} s^2 \left[C_3 e^{(ibs+a|s|)y} + C_4 e^{(ids+c|s|)y}\right] e^{-isx} ds \tag{18}$$

$$\sigma_{xy}^{(-)} = \frac{1}{2\pi}\int_{-\infty}^{\infty} is \left[C_3 (a|s| + ibs) e^{(ibs+a|s|)y} + C_4 (c|s| + ids) e^{(ids+c|s|)y}\right] e^{-isx} ds \tag{19}$$

The continuity conditions for local stresses σ_{yy} and σ_{xy} are identically satisfied, given

$$C_1 + C_2 = C_3 + C_4 \tag{20}$$

and

$$C_1 (bs + ia|s|) + C_2 (ds + ic|s|) = C_3 (bs - ia|s|) + C_4 (ds - ic|s|) \tag{21}$$

respectively.

The solution of equations (20) and (21) for C_3 and C_4 in terms of C_1 and C_2 can be written in the following form:

$$\begin{aligned} C_3 &= S_1 C_1 + S_2 C_2 \\ C_4 &= S_3 C_1 + S_4 C_2 \end{aligned} \tag{22}$$

where

$$\begin{aligned} S_1 &= \frac{|s|(a+c) + i(d-b)s}{|s|(c-a) + i(d-b)s} \\ S_2 &= \frac{2c|s|}{|s|(c-a) + i(d-b)s} \\ S_3 &= -\frac{2a|s|}{|s|(c-a) + i(d-b)s} \\ S_4 &= -\frac{|s|(a+c) - i(d-b)s}{|s|(c-a) + i(d-b)s} \end{aligned} \tag{23}$$

The strains are calculated by using the generalized Hooke's law. The normal strains are

$$\begin{aligned} \varepsilon_{xx} &= b_{11}\sigma_{xx} + b_{12}\sigma_{yy} + b_{16}\sigma_{xy} \\ \varepsilon_{yy} &= b_{12}\sigma_{xx} + b_{22}\sigma_{yy} + b_{26}\sigma_{xy} \end{aligned} \tag{24}$$

From eqs. (24) the strains for the upper and lower half planes can be obtained. Then by using the strain-displacement relations [1]; the displacements for the upper and lower half plane can be obtained:

$$\begin{aligned} u(x,y) &= \int \varepsilon_{xx} dx \\ v(x,y) &= \int \varepsilon_{yy} dy \end{aligned} \tag{25}$$

To obtain the singular integral equations we introduce the following auxiliary functions:

$$f_1(x) = \frac{\partial}{\partial x}[u^+(x,0) - u^-(x,0)] \tag{26}$$

$$f_2(x) = \frac{\partial}{\partial x}[v^+(x,0) - v^-(x,0)] \tag{27}$$

Expressions for the unknown constants C_1 and C_2 can be determined in terms of these auxiliary functions, since we know that $f_1(t)$ and $f_2(t)$ are nonzero only within the crack region (*i.e.*, $-a < t < a$). Therefore,

$$C_1 = \int_{-a}^{a} \frac{D_4 f_1(t) - D_2 f_2(t)}{D_1 D_4 - D_2 D_3} e^{ist} dt \tag{28}$$

$$C_2 = -\int_{-a}^{a} \frac{D_3 f_1(t) - D_1 f_2(t)}{D_1 D_4 - D_2 D_3} e^{ist} dt \tag{29}$$

where

$$\begin{aligned} D_1 &= 2a|s|\left[|s|\,(a+c) + i\,(d-b)\,s\right] b_{11} \\ D_2 &= 2c|s|\left[|s|\,(a+c) - i\,(d-b)\,s\right] b_{11} \\ D_3 &= 2a\frac{|s|s\left[s\,(d-b) - i\,(a+c)\,|s|\right]}{(a^2+b^2)\,(c|s| + ids)} b_{22} \\ D_4 &= 2c\frac{|s|s\left[-s\,(d-b) - i\,(a+c)\,|s|\right]}{(c^2+d^2)\,(a|s| + ibs)} b_{22} \end{aligned} \tag{30}$$

Similarly, C_3 and C_4 can be expressed in terms of the auxiliary functions by using eqs. (22) and the results of eqs. (28) and (29).

Substituting expressions for the constants C_m into the local stress equations (14) through (19) results in the formulation of a set of double integral equations with respect to the Fourier variables s $(-\infty < s < \infty)$ and t $(-a \le t \le a)$. Integrating with respect to s will give a set of singular integral equations with respect to t, which are valid for any jth crack within its own local coordinate system (x_j, y_j) :

$$\sigma^{(j)}_{x_j x_j} = \frac{1}{2\pi}\int_{-a_j}^{a_j}\left[f_{j1}(t_j)\frac{Q_1}{b_{11}Q_0} + f_{j2}(t_j)\frac{Q_2}{b_{22}Q_0}\right] dt_j \tag{31}$$

$$\sigma^{(j)}_{y_j y_j} = \frac{1}{2\pi}\int_{-a_j}^{a_j}\left[f_{j1}(t_j)\frac{Q_3}{b_{11}Q_0} + f_{j2}(t_j)\frac{Q_4}{b_{22}Q_0}\right] dt_j \tag{32}$$

$$\sigma^{(j)}_{x_j y_j} = \frac{1}{2\pi}\int_{-a_j}^{a_j}\left[f_{j1}(t_j)\frac{Q_5}{b_{11}Q_0} + f_{j2}(t_j)\frac{Q_6}{b_{22}Q_0}\right] dt_j \tag{33}$$

where

$$\begin{aligned} Q_0 = {} & ac\left[(a+c)^2 + (b-d)^2\right]\left[(t_j - x_j)^2 + 2b(t_j - x_j)y_j + (a^2+b^2)\,y_j^2\right] \\ & \times \left[(t_j - x_j)^2 + 2d(t_j - x_j)y_j + (c^2+d^2)\,y_j^2\right] \end{aligned} \tag{34}$$

$$Q_1 = R_1\,(t_j - x_j)^3 + y_j\left[R_2\,(t_j - x_j)^2 + y_j R_3\,(t_j - x_j) + y_j^2 R_4\right] \tag{35}$$

with

$$
\begin{aligned}
R_1 &= a^2bc + b^3c + 2abc^2 + 2a^2cd + ac^2d + ad^3 \\
R_2 &= a^4c + 2a^2b^2c + b^4c + 2a^3c^2 + 2ab^2c^2 + 2a^2c^3 + ac^4 \\
&\quad +2a^2bcd + 2b^3cd + 2abc^2d + 2a^2cd^2 + 2ac^2d^2 + 2abd^3 + ad^4 \\
R_3 &= a^2bc^3 + b^3c^3 + 2abc^4 + 2a^4cd + 4a^2b^2cd + 2b^4cd + a^3c^2d \\
&\quad +ab^2c^2d + a^2bcd^2 + b^3cd^2 + 4abc^2d^2 + a^3d^3 + ab^2d^3 + 2abd^4 \\
R_4 &= \left(a^2 + b^2\right)\left(c^2 + d^2\right)\left(a^2c + b^2c + ac^2 + ad^2\right)
\end{aligned}
$$

$$
Q_2 = R_5\left\{(t_j - x_j)^3 R_6 + y_j\left[R_7 (t_j - x_j)^2 - y_j R_8 (t_j - x_j) + y_j^2 R_9\right]\right\} \tag{36}
$$

with

$$
\begin{aligned}
R_5 &= \left(a^2 + b^2\right)\left(c^2 + d^2\right) \\
R_6 &= \left(a^2c + b^2c + ac^2 + ad^2\right) \\
R_7 &= a^2bc + b^3c + 2b^2cd + ac^2d + 2abd^2 + ad^3 \\
R_8 &= a^3c^2 + ab^2c^2 + a^2c^3 - b^2c^3 - 2a^2bcd - 2b^3cd \\
&\quad -2abc^2d - a^3d^2 - ab^2d^2 + a^2cd^2 - b^2cd^2 - 2abd^3 \\
R_9 &= \left(a^2 + b^2\right)\left(c^2 + d^2\right)(bc + ad)
\end{aligned}
$$

$$
Q_3 = R_{10}(t_j - x_j)^3 + y_j\left[-(t_j - x_j)^2 R_{11} + y_j (t_j - x_j) R_{12} + y_j^2 R_{13}\right] \tag{37}
$$

with

$$
\begin{aligned}
R_{10} &= bc + ad \\
R_{11} &= \left(a^2 - b^2\right)c - 2bd(a + c) + a\left(c^2 - d^2\right) \\
R_{12} &= bc^3 + a^3d + ab^2d + bcd^2 + 2bd\,(bc + ad) \\
R_{13} &= \left(a^2 + b^2\right)\left(c^2 + d^2\right)(a + c)
\end{aligned}
$$

$$
Q_4 = R_5\left\{(t_j - x_j)^3 R_{14} + y_j\left[R_{15} (t_j - x_j)^2 + y_j(t_j - x_j)R_{16} + y_j^2 R_{17}\right]\right\} \tag{38}
$$

with

$$
\begin{aligned}
R_{14} &= a + c \\
R_{15} &= 2ab + bc + ad + 2cd \\
R_{16} &= a^3 + ab^2 + 2a^2c + 2ac^2 + c^3 + 2abd + 2bcd + cd^2 \\
R_{17} &= 2abc^2 + bc^3 + a^3d + ab^2d + 2a^2cd + bcd^2
\end{aligned}
$$

$$
Q_5 = R_{18}\,(t_j - x_j)^3 + y_j\left[R_{19}(t_j - x_j)^2 - y_j(t_j - x_j)R_{20} + y_j^2 R_9\right] \tag{39}
$$

with

$$
\begin{aligned}
R_{18} &= c\left(a^2+b^2\right)+a\left(c^2+d^2\right) \\
R_{19} &= a^2bc+b^3c+2b^2cd+ac^2d+2abd^2+ad \qquad (40)\\
R_{20} &= a^3c^2+ab^2c^2+a^2c^3-b^2c^3-2a^2bcd \qquad (41)\\
&\quad -2b^3cd-2abc^2d-a^3d^2-ab^2d^2+a^2cd^2-b^2cd^2-2abd^3
\end{aligned}
$$

and

$$
Q_6 = R_5\left\{(t_j-x_j)^3 R_{21}+y_j\left[R_{22}(t_j-x_j)^2+y_j(t_j-x_j)R_{23}+y_j^2R_{13}\right]\right\} \qquad (42)
$$

with

$$
\begin{aligned}
R_{21} &= ad+bc \\
R_{22} &= -a^2c+b^2c-ac^2+ad^2+2abd+2bcd \\
R_{23} &= bc^3+a^3d+ab^2d+2b^2cd+2abd^2+bcd^2
\end{aligned}
$$

Note, that the special case of an isotropic material can be recovered by the following substitutions: $b=d=0$, and $a=c=1$, thus giving $R_1=R_3=R_7=R_9=R_{10}=R_{12}=R_{15}=R_{17}=R_{19}=R_{21}=R_{23}=0$; $R_5=1$; $R_4=R_6=R_8=R_{11}=R_{13}=R_{14}=R_{18}=R_{20}=-R_{22}=2$; and $R_2=R_{16}=6$. The parameters Q_i then become

$$
Q_0^{(iso)} = 4\left[(t_j-x_j)^2+y_j^2\right]^2 \qquad (43)
$$

$$
Q_1^{(iso)} = 2y_j\left[3(t_j-x_j)^2+y_j^2\right] \qquad (44)
$$

$$
Q_2^{(iso)} = 2(t_j-x_j)\left[(t_j-x_j)^2-y_j^2\right] \qquad (45)
$$

$$
Q_3^{(iso)} = -2y_j\left[(t_j-x_j)^2-y_j^2\right] \qquad (46)
$$

$$
Q_4^{(iso)} = 2(t_j-x_j)\left[(t_j-x_j)^2+3y_j^2\right] \qquad (47)
$$

$$
Q_5^{(iso)} = 2(t_j-x_j)\left[(t_j-x_j)^2-y_j^2\right] = Q_2^{(iso)} \qquad (48)
$$

$$
Q_6^{(iso)} = -2y_j\left[(t_j-x_j)^2-y_j^2\right] = Q_3^{(iso)} \qquad (49)
$$

and the stresses reduce to the isotropic stress formulas derived previously in reference [2].

This completes the formulation of the fundamental problem (or local stress state) for the jth crack. Henceforth, the formulation of the multiple crack problem will be addressed.

4 TOTAL STRESS FORMULATION

The total stress state ${}_p(\sigma^T_{rz})$ for the pth crack is defined as the local stress state of the pth crack (σ^p_{rz}) plus the contribution to that stress state of all remaining cracks. This may be represented mathematically as

$$ {}_p\sigma^T_{rz}(x_p, y_p) = \sigma^p_{rz}(x_p, y_p) + \sum_{j=1}^{n-1} \hat{\sigma}^j_{rz}[x_j(x_p, y_p), y_j(x_p, y_p)] \tag{50} $$

for $p = 1, ..., n$,where $\hat{\sigma}^j_{rz}$ is defined through standard tensor transformation of the stresses, i.e.,

$$ \hat{\sigma}_{rz} = \beta_{lr}\beta_{mz}\sigma_{lm} $$

and β_{lr}, β_{mz} are the direction cosines between the (x_j, y_j) and (x_p, y_p) coordinates with j identifying the remaining cracks. Note, this statement does not imply that the concept of superposition has been invoked, since the stress perturbation boundary conditions (see eqs. (5)) have not yet been utilized to determine the unknown auxiliary functions.

For functional compatibility within eq. (50), coordinate transformations must be simultaneously applied to all remaining jth crack coordinate variables. As a result, the dominant part (i.e., the first term of eq. (50)) possesses a singularity whereas the regular terms within the summation lose their original singularities and yet still contribute to the total stress state, as one might expect.

By replacing subscript j by p in eqs. (33 and 32), respectively, and evaluating them at $y_p = 0$, the singular terms of the singular integral equations are obtained from the first term of eq. (50) applied for shear (σ_{xy}) and for normal stress (σ_{yy}). Finally, the variables x and t are normalized by using $x_p = a_p\xi$ and $t_p = a_p\tau$,where ξ and τ are defined between -1 and 1. Therefore,

$$ \sigma^{(p)}_{x_p y_p} = \frac{1}{\pi}\int_{-1}^{1}\left[E^{p(1)}_{xy}\frac{f_{p1}(\tau_p)}{\tau_p - \xi_p} + E^{p(2)}_{xy}\frac{f_{p2}(\tau_p)}{\tau_p - \xi_p}\right]d\tau_p \tag{51} $$

$$ \sigma^{(p)}_{y_p y_p} = \frac{1}{\pi}\int_{-1}^{1}\left[E^{p(1)}_{yy}\frac{f_{p1}(\tau_p)}{\tau_p - \xi_p} + E^{p(2)}_{yy}\frac{f_{p2}(\tau_p)}{\tau_p - \xi_p}\right]d\tau_p \tag{52} $$

where E_{xy} and E_{yy} are material-related coefficients proportional to local x-direction stiffness (denoted by superscript 1) or local y-direction stiffness (denoted by superscript 2) with respect to the local crack coordinate system. Consequently, we will call them modified stiffness parameters (MSP's). The MSP's are

$$ E^{p(1)}_{xy} = \frac{[c\,(a^2+b^2) + a\,(c^2+d^2)]}{2ac\left[(a+c)^2 + (b-d)^2\right]b_{11}} \tag{53} $$

$$ E^{p(2)}_{xy} = \frac{(a^2+b^2)\,(c^2+d^2)\,(ad+bc)}{2ac\left[(a+c)^2 + (b-d)^2\right]b_{22}} \tag{54} $$

$$ E^{p(1)}_{yy} = \frac{(bc+ad)}{2ac\left[(a+c)^2 + (b-d)^2\right]b_{11}} \tag{55} $$

$$ E^{p(2)}_{yy} = \frac{(a^2+b^2)\,(c^2+d^2)\,(a+c)}{2ac\left[(a+c)^2 + (b-d)^2\right]b_{22}} \tag{56} $$

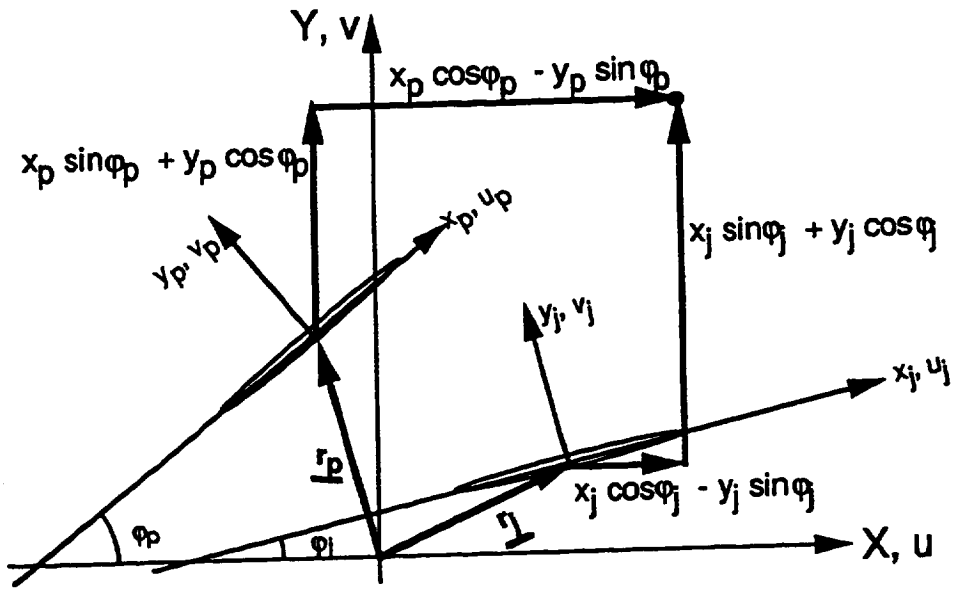

Figure 2: Geometric relationships between a pair of cracks and their local variables.

For the isotropic case

$$E^{p(2)}_{xy} = E^{p(1)}_{yy} = 0$$

and

$$E^{p(1)}_{xy} = E^{p(2)}_{yy} = \frac{E}{4} \tag{57}$$

whereas in the orthotropic case, only

$$E^{p(2)}_{xy} = E^{p(1)}_{yy} = 0$$

The regular terms of the singular integral equations are obtained by transforming the remaining stresses into the local pth crack coordinate system simultaneously with coordinate transformation. The coordinate transformation between the x_j, y_j and x_p, y_p systems is determined from the following geometric relationship (see Fig. 2):

$$r_{jX} + x_j cos\varphi_j - y_j sin\varphi_j = r_{pX} + x_p cos\varphi_p - y_p sin\varphi_p \tag{58}$$

$$r_{jY} + x_j sin\varphi_j + y_j cos\varphi_j = r_{pY} + x_p sin\varphi_p + y_p cos\varphi_p \tag{59}$$

where r_{jX}, r_{jY} are the rectangular components of the jth crack position vector referred to the global coordinate system $X-Y$, and φ_j is the angle of rotation between the global and local systems.

One component of the regular part of the total stress is obtained by transformation of the stresses from jth crack local coordinate system into the pth crack local coordinate system simultaneously with the coordinate transformation and substituting $y_p = 0$:

$$\begin{aligned} \hat{\sigma}^j_{x_p y_p} &= -\left(\sigma^{(j)}_{x_j x_j} - \sigma^{(j)}_{y_j y_j}\right) \sin\theta\cos\theta + \sigma^{(j)}_{x_j y_j}\left(\cos^2\theta - \sin^2\theta\right) \\ \hat{\sigma}^j_{y_p y_p} &= \sigma^{(j)}_{x_j x_j} \sin^2\theta + \sigma^{(j)}_{y_j y_j} \cos^2\theta - 2\sigma^{(j)}_{x_j y_j} \sin\theta\cos\theta \end{aligned} \tag{60}$$

where $\theta = \varphi_p - \varphi_j$. Therefore, we can obtain from eqs. (58) and (59)

$$\begin{aligned} x_j &= p_1 + x_p \cos\theta \\ y_j &= p_2 + x_p \sin\theta \end{aligned} \tag{61}$$

where $(p1, p2)$ is the vector connecting the centers from jth to pth cracks expressed in the jth coordinate system:

$$\begin{aligned} p_1 &= (r_{pY} - r_{jY}) \sin\varphi_j + (r_{pX} - r_{jX}) \cos\varphi_j \\ p_2 &= (r_{pY} - r_{jY}) \cos\varphi_j - (r_{pX} - r_{jX}) \sin\varphi_j \end{aligned} \tag{62}$$

The regular, normalized form of the parameters Q_i for $i = 0, 1, ..., 6$ is obtained by using the coordinate normalization $x_p = a_p\xi$ and $t_j = a_j\tau$, in addition to the coordinate transformation, to produce the parameters $Q_i^{(reg)}$:

$$\begin{aligned} Q_0^{(reg)} = \; & ac\left[(a+c)^2 + (b-d)^2\right]\left[(a_j\tau - p_1 - a_p\xi\cos\theta)^2 + \right. \\ & 2b(a_j\tau - p_1 - a_p\xi\cos\theta)(p_2 + a_p\xi\sin\theta) + (a^2+b^2)(p_2 + a_p\xi\sin\theta)^2\Big] \\ & \Big[(a_j\tau - p_1 - a_p\xi\cos\theta)^2 + 2d(a_j\tau - p_1 - a_p\xi\cos\theta)(p_2 + a_p\xi\sin\theta) + \\ & \left.(c^2+d^2)(p_2 + a_p\xi\sin\theta)^2\right] \end{aligned} \tag{63}$$

$$\begin{aligned} Q_1^{(reg)} = \; & R_1(a_j\tau - p_1 - a_p\xi\cos\theta)^3 + (p_2 + a_p\xi\sin\theta)\left[R_2(a_j\tau - p_1 - a_p\xi\cos\theta)^2\right. \\ & \left. + (p_2 + a_p\xi\sin\theta)R_3(a_j\tau - p_1 - a_p\xi\cos\theta) + (p_2 + a_p\xi\sin\theta)^2 R_4\right] \end{aligned} \tag{64}$$

$$\begin{aligned} Q_2^{(reg)} = \; & \Big\{(a_j\tau - p_1 - a_p\xi\cos\theta)^3 R_6 + (p_2 + a_p\xi\sin\theta)\left[R_7(a_j\tau - p_1 - a_p\xi\cos\theta)^2\right. \\ & \left. - (p_2 + a_p\xi\sin\theta)R_8(a_j\tau - p_1 - a_p\xi\cos\theta) + (p_2 + a_p\xi\sin\theta)^2 R_9\right]\Big\} R_5 \end{aligned} \tag{65}$$

$$\begin{aligned} Q_3^{(reg)} = \; & R_{10}(a_j\tau - p_1 - a_p\xi\cos\theta)^3 + (p_2 + a_p\xi\sin\theta)\left[-(a_j\tau - p_1 - a_p\xi\cos\theta)^2 R_{11}\right. \\ & \left. + (p_2 + a_p\xi\sin\theta)(a_j\tau - p_1 - a_p\xi\cos\theta)R_{12} + (p_2 + a_p\xi\sin\theta)^2 R_9\right] \end{aligned} \tag{66}$$

$$\begin{aligned} Q_4^{(reg)} = \; & \Big\{(a_j\tau - p_1 - a_p\xi\cos\theta)^3 R_{14} + (p_2 + a_p\xi\sin\theta)\left[R_{15}(a_j\tau - p_1 - a_p\xi\cos\theta)^2\right. \\ & \left. + (p_2 + a_p\xi\sin\theta)(a_j\tau - p_1 - a_p\xi\cos\theta)R_{16} + (p_2 + a_p\xi\sin\theta)^2 R_{17}\right]\Big\} R_5 \end{aligned} \tag{67}$$

$$\begin{aligned} Q_5^{(reg)} = \; & R_{18}(a_j\tau - p_1 - a_p\xi\cos\theta)^3 + (p_2 + a_p\xi\sin\theta)\left[R_{19}(a_j\tau - p_1 - a_p\xi\cos\theta)^2\right. \\ & \left. - (p_2 + a_p\xi\sin\theta)(a_j\tau - p_1 - a_p\xi\cos\theta)R_{20} + (p_2 + a_p\xi\sin\theta)^2 R_9\right] \end{aligned} \tag{68}$$

$$\begin{aligned} Q_6^{(reg)} = \; & \Big\{(a_j\tau - p_1 - a_p\xi\cos\theta)^3 R_{21} + (p_2 + a_p\xi\sin\theta)\left[R_{22}(a_j\tau - p_1 - a_p\xi\cos\theta)^2\right. \\ & \left. + (p_2 + a_p\xi\sin\theta)(a_j\tau - p_1 - a_p\xi\cos\theta)R_{23} + (p_2 + a_p\xi\sin\theta)^2 R_{13}\right]\Big\} R_5 \end{aligned} \tag{69}$$

So the regular normalized component of the shear stress becomes

$$\hat{\sigma}^j_{x_p y_p} = \int_{-1}^{1} \ker_1 f_{j1}(t_j) d\tau_j + \int_{-1}^{1} \ker_2 f_{j2}(t_j) d\tau_j \tag{70}$$

where

$$\ker_1 = \frac{a_j}{2\pi} \frac{1}{b_{11} Q_0^{(reg)}} \left[- \left(Q_1^{(reg)} - Q_3^{(reg)} \right) \sin\theta \cos\theta + Q_5^{(reg)} \left(\cos^2\theta - \sin^2\theta \right) \right] \tag{71}$$

$$\ker_2 = \frac{a_j}{2\pi} \frac{1}{b_{22} Q_0^{(reg)}} \left[- \left(Q_2^{(reg)} - Q_4^{(reg)} \right) \sin\theta \cos\theta + Q_6^{(reg)} \left(\cos^2\theta - \sin^2\theta \right) \right] \tag{72}$$

The regular normalized component of normal stress is

$$\hat{\sigma}^j_{y_p y_p} = \int_{-1}^{1} \ker_3 f_{j1}(t_j) d\tau_j + \int_{-1}^{1} \ker_4 f_{j2}(t_j) d\tau_j \tag{73}$$

where

$$\ker_3 = \frac{a_j}{2\pi} \frac{1}{b_{11} Q_0^{(reg)}} \left[Q_1^{(reg)} \sin^2\theta + Q_3^{(reg)} \cos^2\theta - 2 Q_5^{(reg)} \sin\theta \cos\theta \right] \tag{74}$$

$$\ker_4 = \frac{a_j}{2\pi} \frac{1}{b_{22} Q_0^{(reg)}} \left[Q_2^{(reg)} \sin^2\theta + Q_4^{(reg)} \cos^2\theta - 2 Q_6^{(reg)} \sin\theta \cos\theta \right] \tag{75}$$

Thus, the total stresses (σ^T_{yy} and σ^T_{xy}) for n cracks can be written in the following form:

$$\begin{aligned} {}_n\sigma^T_{xy} = \Big\{ & \textstyle\int_{-1}^{1} \ker{}_1 f_{11} d\tau + \int_{-1}^{1} \ker{}_2 f_{12} d\tau + \ldots + \int_{-1}^{1} \ker{}_1 f_{(n-1)1} d\tau \\ & + \textstyle\int_{-1}^{1} \ker{}_2 f_{(n-1)2} d\tau + \frac{E^{n(1)}_{xy}}{\pi} \int_{-1}^{1} \frac{f_{n1}}{\tau - \xi} d\tau + \frac{E^{n(2)}_{xy}}{\pi} \int_{-1}^{1} \frac{f_{n2}}{\tau - \xi} d\tau \Big\} \end{aligned} \tag{76}$$

$$\begin{aligned} {}_n\sigma^T_{yy} = \Big\{ & \textstyle\int_{-1}^{1} \ker{}_3 f_{11} d\tau + \int_{-1}^{1} \ker{}_4 f_{12} d\tau + \ldots + \int_{-1}^{1} \ker{}_3 f_{(n-1)1} d\tau \\ & + \textstyle\int_{-1}^{1} \ker{}_4 f_{(n-1)2} d\tau + \frac{E^{n(1)}_{yy}}{\pi} \int_{-1}^{1} \frac{f_{n1}}{\tau - \xi} d\tau + \frac{E^{n(2)}_{yy}}{\pi} \int_{-1}^{1} \frac{f_{n2}}{\tau - \xi} d\tau \Big\} \end{aligned} \tag{77}$$

The formulation of this system of singular integral equations is complete once the single-value conditions for the auxiliary functions $f_{j\eta}$ are chosen. In the case of straight cracks, this single-value condition [3] is

$$\int_{-1}^{1} f_{j\eta}(\tau) d\tau = 0 \tag{78}$$

where j stands for the jth crack, and η takes on the value of 1 or 2.

5 SOLUTION FOR THE STRESS INTENSITY FACTORS

The integral equations obtained are of the Cauchy type; thus for sharp cracks, the stresses and strains will have a square-root singularity, and the classic definition of a SIF may be used (see refs. [4], [5], [6] and [7]). Therefore, the mode I and II SIF's for the jth crack are

$$k_1^j(1) = \lim_{\xi \to 1}[2(\xi - 1)]^{\frac{1}{2}} \left\{ {}_j\sigma_{yy}^T(\xi, 0) \right\} \tag{79}$$

$$k_2^j(1) = \lim_{\xi \to 1}[2(\xi - 1)]^{\frac{1}{2}} \left\{ {}_j\sigma_{xy}^T(\xi, 0) \right\} \tag{80}$$

$$k_1^j(-1) = \lim_{\xi \to -1}[-2(1 + \xi)]^{\frac{1}{2}} \left\{ {}_j\sigma_{yy}^T(\xi, 0) \right\} \tag{81}$$

$$k_2^j(-1) = \lim_{\xi \to -1}[-2(1 + \xi)]^{\frac{1}{2}} \left\{ {}_j\sigma_{xy}^T(\xi, 0) \right\} \tag{82}$$

where the normal and shear stresses, eqs. (76) and (77), are used. Note that this definition of a SIF was originally developed for an isotropic material wherein the mode-I normal stress is related only to the normal crack-opening displacement Δv and the mode-II shear stress is related only to the shear displacement Δu. The same definition can also be applied to anisotropic materials by assuming that modes I and II are based on normal and shear stresses only; however, as will be shown in eqs. (86) to (89), these stresses are driven by a mixed mode displacement (Δv and Δu) field.

It is well known [3] that the auxiliary functions (f) can be expressed as a product of the unknown bounded functions (H) and the known singular weight functions (w):

$$f(\tau) = H(\tau)w(\tau) \tag{83}$$

The singular weight function w for a sharp crack is

$$w(\tau) = (\tau^2 - 1)^{-\frac{1}{2}} \tag{84}$$

Erdogan [3] found, for example, that in the case of a Cauchy-type singular integral equation (eqs. (76) and (77)), the dominant part can be expressed in terms of the function H evaluated at the tips of the jth crack:

$$\frac{1}{\pi}\int_{-1}^{1} \frac{f_{\eta j} d\tau}{\tau - \xi} = H_{\eta j}(-1)\frac{e^{i\pi/2}}{\sqrt{2}}(\tau + 1)^{-\frac{1}{2}} - H_{\eta j}(1)\frac{1}{\sqrt{2}}(\tau - 1)^{-\frac{1}{2}} + O(\tau) \tag{85}$$

where η is 1 or 2, and $O(\tau)$ is the higher order term, which in subsequent calculations is neglected. Equations (85) can be substituted for the dominant part (last two terms in eqs. (76) and (77)) of the normal and shear components of the total stresses in eqs. (79) to (82). This substitution and subsequent evaluation of the limits at the crack tips results in the redefining of the SIF's, normalized with respect to $\sqrt{a_1}$ and σ_{jp}^o, and expressed in terms of the functions $H_{\eta j}$:

$$k_1^j(1) = \left[E_{yy}^{j(1)} H_{1j}(1) + E_{yy}^{j(2)} H_{2j}(1) \right] \sqrt{a_j/a_1} \tag{86}$$

$$k_2^j(1) = \left[E_{xy}^{j(1)} H_{1j}(1) + E_{xy}^{j(2)} H_{2j}(1) \right] \sqrt{a_j/a_1} \tag{87}$$

$$k_1^j(-1) = -\left[E_{yy}^{j(1)} H_{1j}(-1) + E_{yy}^{j(2)} H_{2j}(-1) \right] \sqrt{a_j/a_1} \tag{88}$$

$$k_2^j(-1) = -\left[E_{xy}^{j(1)} H_{1j}(-1) + E_{xy}^{j(2)} H_{2j}(-1) \right] \sqrt{a_j/a_1} \tag{89}$$

The Lobatto-Chebyshev collocation integration technique was employed, because it is known to provide excellent results in dealing with the preceding Cauchy-type singular

integral equations. The unknown functions $H_{\eta j}$ are determined at a discrete set of points $\tau_1, \tau_2, ..., \tau_m$ called abscissas. In this way, each integral equation is reduced to a set of algebraic equations with unknowns $H_{\eta j}(\tau_1)$, $H_{\eta j}(\tau_2)$, ..., $H_{\eta j}(\tau_m)$, which are the discrete values of the functions $H_{\eta i}$; hence its name, discrete auxiliary function. Note that H_{1j} and H_{2j} are proportional, respectively, to the difference in shear and normal displacements at the crack tips:

$$\begin{aligned} \Delta u &\sim H_1 \\ \Delta v &\sim H_2 \end{aligned} \tag{90}$$

Consequently, $H_{\eta j}$ can be used as a measure of the crack-opening displacement at the crack tip.

Each of the singular integral equations subjected to the stress boundary conditions (eqs. 5) can be replaced by $m-1$ algebraic equations with 2nm unknown parameters (see ref. [2]).In the Lobatto-Chebyshev method, the abscissas are calculated according to

$$\tau_r = \cos\frac{(r-1)\pi}{m-1} \quad \text{for} \quad r = 1, ..., m \tag{91}$$

with the corresponding weights given by

$$w_1 = w_m = \frac{\pi}{2(m-1)} \quad \text{and} \quad w_r = \frac{\pi}{m-1} \quad \text{for} \quad r = 2, 3, ..., m-1 \tag{92}$$

The collocation points are then found by using the formula

$$\xi_z = \cos\frac{(2z-1)\pi}{2m-2} \quad \text{for} \quad z = 1, 2, ..., m-1 \tag{93}$$

In order to have the complete system of $2nm$ algebraic equations, the single-value conditions (eqs.(78)) are also expressed by using the collocation technique:

$$\sum_{r=1}^{m} H_{\eta j}(\tau_r) w_r = 0 \tag{94}$$

Thus, the resulting system of algebraic equations can be written in the form

$$[A]\{H\} = \{\mathcal{R}\} \tag{95}$$

where [A] is a fully populated $2nm \times 2nm$ matrix of coefficients and $\{\mathcal{R}\}$ is the loading function vector.

The unknown parameter vector $\{H\}$ can be determined through inversion of the [A] matrix; thus,

$$\{H\} = [A]^{-1}\{\mathcal{R}\} \tag{96}$$

although only the appropriate values (*i.e.*, $H_{\eta j}(\pm 1)$) are used to calculate the SIF's for the jth crack (see eqs. (86) to (89)).

The general solution for any multicrack problem is now complete with the automatic generation of the associated FORTRAN code for the evaluation of eqs. (96). This FORTRAN program was utilized to obtained the following results, which are compared with published results obtained by other methods.

6 STRAIN ENERGY RELEASE RATE

In fracture mechanics, perhaps the most important physical quantity is the strain energy release rate (G_T), usually denoted by G. Cherepanov[8] discussed the generalized formula for G_T given an anisotropic material.

$$G = \frac{1}{2}\int_a^{a+da} \left\{ \sigma_{yy}^T(x,0)\left[v(x-da,0^+) - v(x-da,0^-)\right] + \sigma_{xy}^T(x,0)\left[u(x-da,0^+) - u(x-da,0^-)\right] \right\} dx \tag{97}$$

Using the roots of the characteristic equation in terms of the real components eq. (11), we can show that

$$G_T = \frac{\pi}{2}\left[k_1^2 \frac{(a+c)(ac-bd) + (b+d)(ad+bc)}{(ac-bd)^2 + (ad+bc)^2} b_{22} + k_2^2 (a+c) b_{11} \right] \tag{98}$$

or utilizing eqs. (102) and (105), developed subsequently, we can obtain a simplified expression for G_T, that is

$$G_T = \frac{\pi}{2} K_{eff}^2 (a+c) b_{11} \tag{99}$$

where

$$K_{eff} = \sqrt{k_1^2 \frac{E_{xy}^{(1)}}{E_{yy}^{(2)}} + k_2^2}$$

and represents an effective SIF. Note the significant coupling between the normal and shear stresses and the displacement components in this effective SIF.

In the case of an isotropic material we may substitute $a = c = 1$, $b = d = 0$, $E_{xy}^{(1)} = E_{yy}^{(2)}$, and $b_{11} = b_{22} = \frac{1}{E}$ into eq. (98). Consequently, the well-known fracture mechanics relationship is recovered:

$$G^{(iso)} = \frac{\pi}{E}\left\{ \left[k_1^{(iso)}\right]^2 + \left[k_2^{(iso)}\right]^2 \right\} \tag{100}$$

7 NUMERICAL APPLICATIONS

The focus of the following parametric study will be limited to investigating the influence of the crack geometry configuration and strength of anisotropy on the resulting driving force. To accomplish this the four independent elastic constants were taken to be

$$\begin{aligned} \frac{G_{LT}}{E_{TT}} &= 0.4 \\ \nu_{LT} &= 0.25 \\ \frac{E_{TT}}{E_{TT}} &= 1.0 \end{aligned}$$

and the strength of anisotropy, $\frac{E_{LL}}{E_{TT}}$, is a specified constant greater than or equal to one. Note that E_{TT} is always chosen to be the weaker direction, i.e., to be less than or equal to E_{LL}. Although, the influence of G_{LT} and ν_{LT} on the driving force is important, this aspect of the parametric study will be reserved for future work.

7.1 *Two Crack Interaction*

7.1.1 *Collinear Cracks*

In order to validate the results obtained with the automatically generated FORTRAN code, the well-known problem of two parallel interacting cracks is considered here. The plate, with two cracks of length $2a$ and a preferred direction defined by $\Omega = 22°$, is subjected to a normal far-field stress state (σ°_{YY}) as shown in Fig. 3. Results are obtained

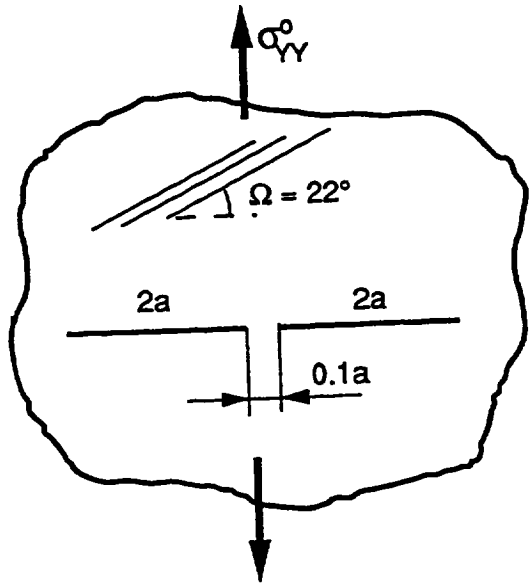

Figure 3: Geometry and loading condition of two collinear cracks problem.

over a wide range of strengths of anisotropy, as defined by the ratio E_{LL}/E_{TT}. As Fig. 4 shows, the SIF's do not depend on the strength of anisotropy, even though the discrete auxiliary functions do. The results indicate that at both the inner and outer crack tips mode-I SIF's are exactly the same as the isotropic SIF's from references [9] and [11], and mode-II SIF's are zero for this configuration.

Although, the mode-II SIF is zero over the entire range of strengths of anisotropy examined, the shear crack opening, as represented by H_1 (see eq. (90) is zero only for the special case of an isotropic material (i.e., $E_{LL}/E_{TT} = 1$). Figure 4 clearly shows that even small amounts of anisotropy ($E_{LL}/E_{TT} > 1$) produce shear displacements at the crack tip and that this shear displacement increases significantly for $1 < E_{LL}/E_{TT} < 5$ and becomes constant for $E_{LL}/E_{TT} > 15$. Consequently, two collinear cracks within a transversely isotropic material will always (provided $\Omega = 22°$) produce a mode-I crack tip local stress field with a **mixed-mode** local displacement field even when the strength of anisotropy is small. This fact can be understood, even for the case of a single crack[10], by examining eqs. (86) to (89), where it is apparent that in an anisotropic material the normal and shear stresses are coupled with both normal and shear displacement components, respectively.

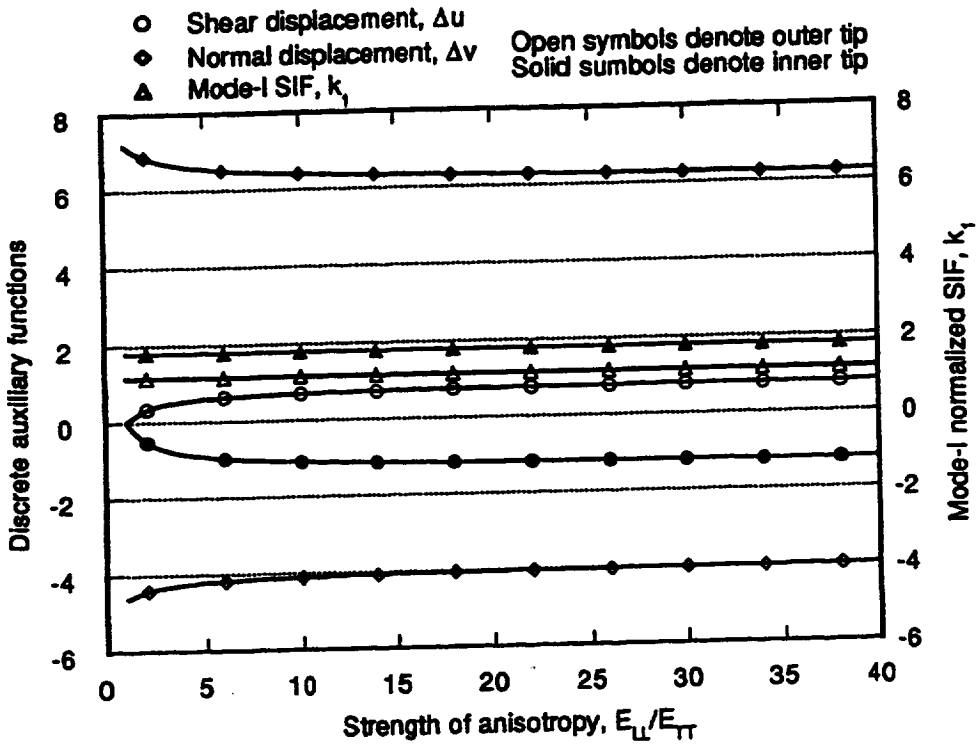

Figure 4: Discrete auxiliary functions and normalized SIF's versus strength of anisotropy E_{LL}/E_{TT} for two equal collinear cracks in a composite plate reinforced at $\Omega = 22°$ and subjected to far-field normal stress, see Fig. 3.

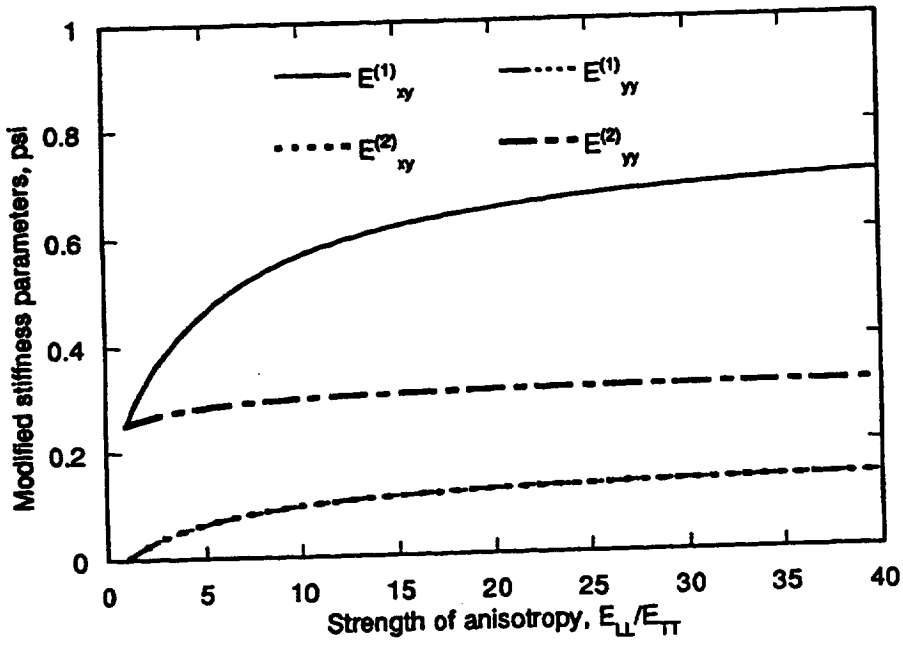

Figure 5: Modified stiffness parameters versus strength of anisotropy E_{LL}/E_{TT} for two equal collinear cracks in a composite plate reinforced at $\Omega = 22°$ and subjected to far-field normal stress, see Fig. 3.

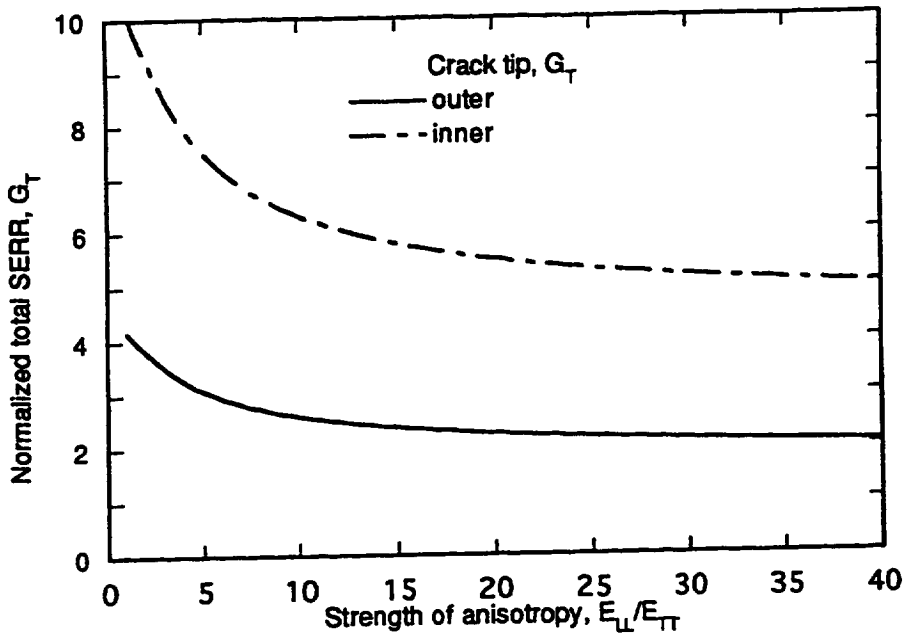

Figure 6: Normalized G_T versus strength of anisotropy E_{LL}/E_{TT} for two equal collinear cracks in a composite plate (reinforced at $\Omega = 22°$; and subjected to far-field normal stress, see Fig. 3).

Figure 5 shows how the MSP's vary with respect to the strength of anisotropy E_{LL}/E_{TT}. Using the isotropic values (i.e., $E_{LL}/E_{TT} = 1$) of the MSP's, we can obtain the results given in equation (57). Increasing the strength of anisotropy significantly increases $E^{(1)}_{xy}$, $E^{(2)}_{xy}$ and $E^{(1)}_{yy}$, while $E^{(2)}_{yy}$ remains nearly constant. Note that $E^{(2)}_{xy} = E^{(1)}_{yy}$ over the entire range of E_{LL}/E_{TT}. Revisiting eq. (87) and Figs 4 and 5, explains why the mode II SIF is zero. It stems from the fact that although both normal and shear displacements are induced, $E^{(2)}_{xy}$ is so much less than $E^{(1)}_{xy}$ that the influences of the normal and shear displacements are counteracted.

As discussed previously, the total G_T represents an important measure of the driving force for crack propagation in fracture mechanics. The G_T's at the inner and outer crack tips for the two collinear cracks are shown in Fig. 6. Clearly, the maximum G_T's (for both the inner and outer crack tips) occur in the isotropic case. In the anisotropic case when $E_{LL}/E_{TT} > 15$ the G_T's rapidly reduce to nearly 50% of the isotropic values. Although both the G_T (Fig. 6) and the SIF's (Fig. 4) indicate that the inner crack tip will propagate, only the G_T's unambiguously indicate that as the strength of anisotropy increases, the crack-driving force is reduced. Thus, we can conclude that (1) the isotropic case gives rise to the greatest driving force and (2) that the SIF (unlike the G_T) is unable to detect the decrease in the crack-driving force as a function of strength of anisotropy.

Now let us examine the influence of changing the preferred direction angle Ω on the same collinear crack configuration with a strength of anisotropy ratio $E_{LL}/E_{TT} = 40$. Results shown in Fig. 7 indicate that the mode-I SIF's are the same as those previously obtained, even though the discrete auxiliary functions show that the normal and shear crack-opening displacements vary significantly with preferred direction. Note that the

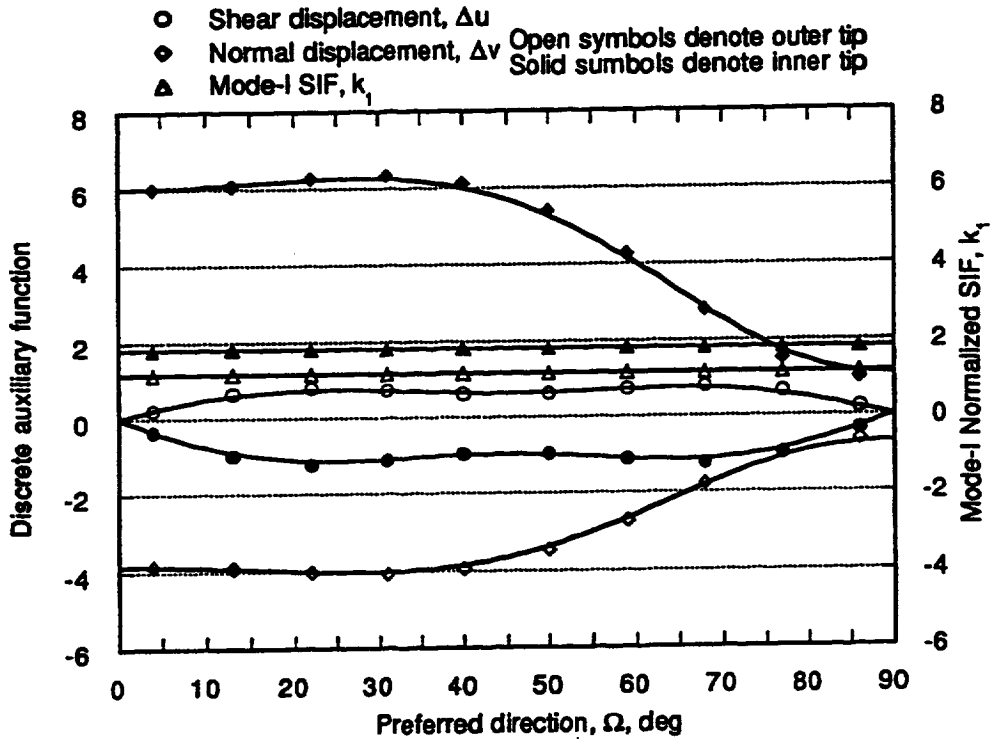

Figure 7: Discrete auxiliary functions and normalized SIF's versus Ω for two equal collinear cracks in a composite plate (strength of anisotropy $E_{LL}/E_{TT} = 40$; subjected to far-field normal stress,see Fig. 3).

shear displacements are zero only for the special cases in which the preferred direction is parallel ($\Omega = 0°$) or normal ($\Omega = 90°$) to the crack configuration; otherwise both openings have nonzero values. The local shear crack-opening displacements maxima occur at $\Omega = 22°$ and $68°$, whereas the local nonzero minimum for the shear displacement occurs at $\Omega = 45°$. Conversely, the normal crack-opening displacements are approximately constant over the range $0 < \Omega < 40$ with the maximum value occurring at $\Omega = 30°$; it then significantly decreases when $\Omega > 40$, until a value equivalent to 30% of the maximum normal opening is reached at $\Omega = 90°$. Clearly, this indicates that although mixed mode-displacements may be observed, in actuality, counter to common expectations resulting from isotropic materials, the anisotropic case may have only a mode-I driving force.

In Figure 8 the MSP's are shown as a function of the preferred direction orientation angle Ω. Note that the $E^{(1)}_{xy}$ curve relative to the curve $E^{(2)}_{yy}$ is symmetrical about the line $\Omega = 45°$. The other two MSP's are again equal to each other and to zero for the orthogonal cases $\Omega = 0°$ and $90°$. Consequently, $E^{(1)}_{xy}$ and $E^{(2)}_{yy}$ must be related to b_{16} and b_{26} (see eq. (9)). In order to give a clearer physical interpretation to $E^{(1)}_{xy}$ and $E^{(2)}_{yy}$ let us relate them to the corresponding material parameters E_{LL} and E_{TT}.

Considering the fact that

$$E^{(2)}_{xy} = E^{(1)}_{yy} \tag{101}$$

we can substitute eqs. (54) and (55) into eq. (101) and solve for b_{22}:

$$b_{22} = b_{11}\left(a^2 + b^2\right)\left(c^2 + d^2\right) \tag{102}$$

Or in terms of the roots of the characteristic equation

$$\mu_1\mu_2\mu_3\mu_4 = \frac{b_{22}}{b_{11}} \tag{103}$$

In the case of a transversely isotropic or orthotropic material, $b = d = 0$, so eq. (103) reduces to a well-known mathematical relation of the following form:

$$a^2c^2 = \frac{E_{LL}}{E_{TT}} \tag{104}$$

By substituting eq. (102) into eq. (56), and the resulting equation into eq. (53), we find that

$$E^{(1)}_{xy} = E^{(2)}_{yy}\frac{c\left(a^2 + b^2\right) + a\left(c^2 + d^2\right)}{(a + c)} \tag{105}$$

Thus, by using eq. (104) together with the transversely isotropic or orthotropic form of eq. (105) (i.e., $b = d = 0$) we can show that

$$\left[\frac{E^{(1)}_{xy}}{E^{(2)}_{yy}}\right]_{b=d=0} = ac = \sqrt{\frac{E_{LL}}{E_{TT}}} \tag{106}$$

On the basis of eq. (106) and our observations from Fig. 8 we may conclude that for the general anisotropic case, $E^{(1)}_{xy}$ is proportional to the square root of the effective Young's modulus in the local $x-$direction and $E^{(2)}_{yy}$ is proportional to the square root of the effective Young's modulus in the local $y-$direction. Note, however, for the general anisotropic case the constants of proportionality are interdependent.

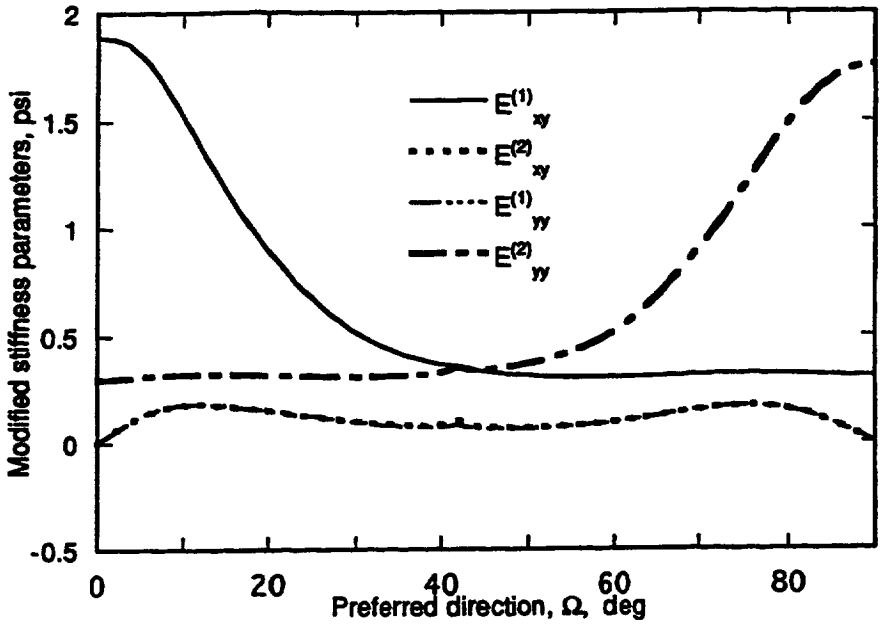

Figure 8: Modified stiffness parameters versus Ω for two equal collinear cracks in a composite plate (strength of anisotropy $E_{LL}/E_{TT} = 40$; subjected to far-field normal stress, see Fig. 3).

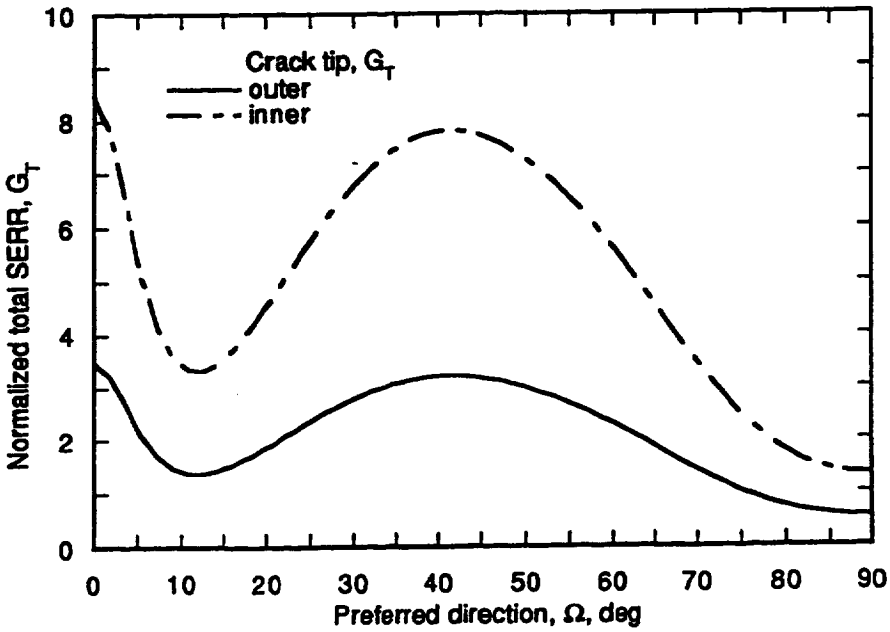

Figure 9: Normalized G_T versus Ω for two equal collinear cracks in a composite plate (strength of anisotropy $E_{LL}/E_{TT} = 40$; subjected to far-field normal stress, see Fig. 3).

The importance of being able to use the G_T as a damage propagation criterion is once again illustrated in Fig. 9, which shows the total G_T versus the orientation angle Ω. Clearly, there are a number of angles at which G_T extrema exist. The global maximum occurs at $\Omega = 0°$, and the global minimum at $\Omega = 90°$, for both inner and outer crack tips. The other two important angles at which the G_T's reach a local minimum and maximum are $\Omega = 12°$ and $\Omega = 42°$, respectively. Again a comparison of Figs. 7 and 9 shows that the G_T's can indicate the critical angles of interest, whereas the SIF's are completely insensitive to variation of the preferred direction.

7.1.2 Parallel cracks

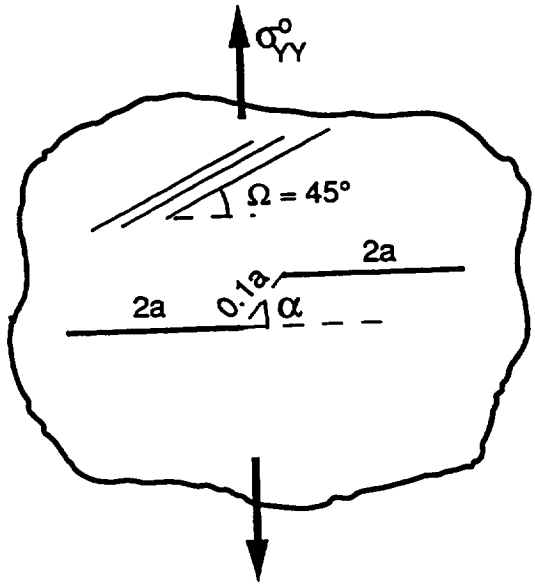

Figure 10: Geometry and loading condition defining two parallel crack problem.

Now let us consider the variation of the SIF's, the crack-opening displacements, and the G_T's for the case when the two cracks are not collinear. A convenient parameter that can be controlled is the inclination angle designated α between the horizontal axis and the line connecting the inner crack tips in Fig. 10. An example of the previous case (collinear cracks) is easily obtained by setting $\alpha = 0°$. The constant parameters are the distance between inner crack tips, $0.1a_1$(where $2a_1$ is the crack length of crack number 1), the strength of anisotropy $E_{LL}/E_{TT} = 40$; and the preferred direction $\Omega = 45°$. As a result of changing the crack configuration, the SIF's are no longer constant for the inner crack tips; those associated with the outer crack tips, however, are not significantly influenced. As illustrated in Fig. 11, mode-I SIF for the inner crack tip monotonically increases with the angle α; whereas mode-II SIF is zero only for $\alpha = 0°$ and $90°$ and attains a maximum at $\alpha = \Omega = 45°$, as we might expect.

It is interesting to analyze the discrete auxiliary functions which approximate the shear and normal crack-opening displacements, Δu and Δv. The shear term of the inner

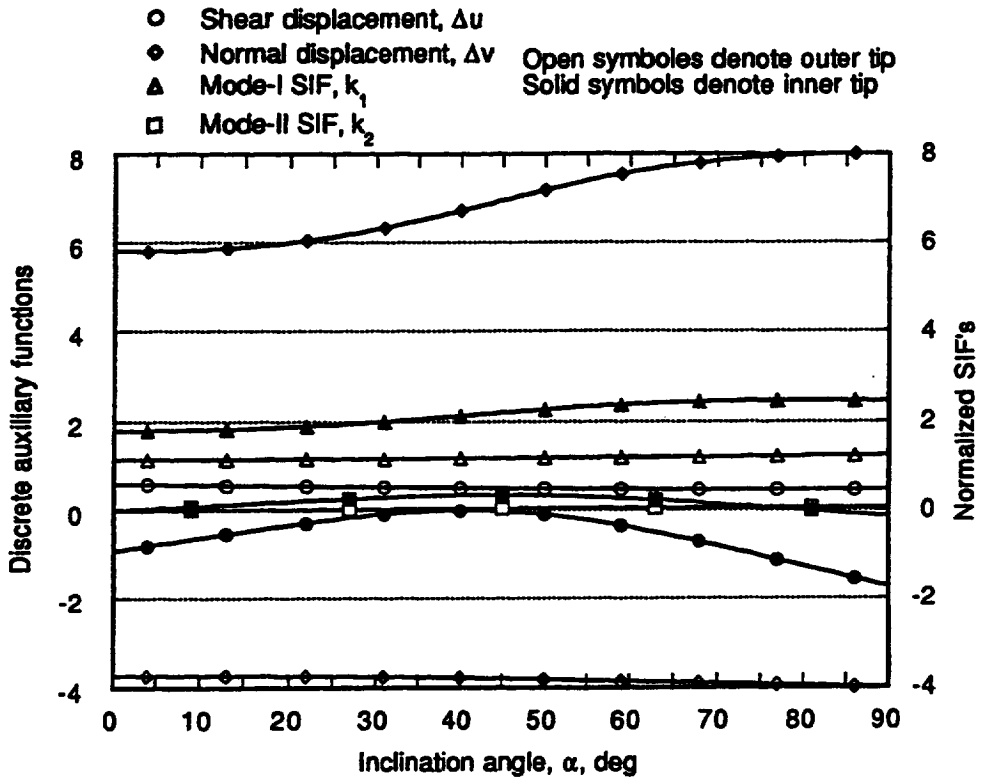

Figure 11: Discrete auxiliary functions and normalized SIF's versus α for two equal non-collinear cracks in a composite plate (strength of anisotropy $E_{LL}/E_{TT} = 40$; reinforced at $\Omega = 45°$; subjected to far-field normal stress, see Fig. 10).

crack tip is zero only when $\alpha = 40°$(even though the shear stress is at a maximum). It is larger for this configuration at $\alpha = 90°$ (when the shear stress is zero) than it is for the collinear crack configuration. Normal crack-opening displacements are the largest also for $\alpha = 90°$. Note that changing the crack configuration by changing α does not change the material properties because they are defined in the local coordinate system; therefore, given the preferred direction $\Omega = 45°$ we can find the pertinent MSP's in Fig. 8.

Once again the combined effect of mode-I and -II SIF's and the normal and shear local displacements are captured by the single scalar measure known as the G_T (see eq. (97)). Figure 12 shows the G_T at both the inner and outer crack tips as a function of the crack configuration angle α. The shapes of these curves resemble the shapes of k_1 and k_2 for the inner crack tips (the degree of influence that k_1 and k_2 have on the G_T is clearly shown in eq. (99)). Since the maximum values of k_1 and k_2 are reached at 90° and 45°, respectively, the maximum value of the G_T would be expect to occur somewhere in between. Figure 12 indicates that for the inner crack tips this maximum is reached when $\alpha = 70°$; however, at the outer crack tip the G_T is only slightly affected (as are k_1 and k_2) by a change in α, and it reaches its maximum when $\alpha = 90°$.

7.1.3 Nonparallel Cracks

Consider a related case wherein the material strength of anisotropy is $E_{LL}/E_{TT} = 40$, the preferred direction is denoted by $\Omega = 30°$, and the two cracks of equal length are configured as shown in the Fig. 13. This figure indicates that crack *ab* remains horizontal, while crack *cd* rotates around the crack tip *c*; where the crack tip distance between tips *b* and *c* remains constant. Here we will examine the influence of varying the angular orientation of crack *cd*, $\phi(2)$, from 0 to 180°. Figures 14 and 15 show the mode-I and -II SIF's, respectively, at the four crack tips. Notice that the outer crack tip of the horizontal crack (tip *a*) is only slightly affected by the change in angular orientation of the crack *cd*. Whereas, the other crack tips (*b*, *c*, and *d*) display significant and complex interactive behavior for both mode-I and -II SIF. For example, mode-I SIF for crack tip b has a local maximum at 21, 42 and 132°, and a local minimum at 0, 31, 122, and 180°, while crack tip *c* starts at the same value as tip *b*, then smoothly decreases to approximately zero (within the range $80 < \phi(2) < 140°$) whereupon the SIF sharply rises to again the same value of SIF as that of crack tip *a*, at $\phi(2) = 180°$. Similarly, extremum are observed for the mode-II SIF at a variety of angle, that is 20, 43, 110, 120 and 132°.

The actual calculated G_T's are shown in Fig. 16. By comparing Fig.16 to Figs. 14 and 15, we can observe that the location of the extremum for the G_T's are similar to the SIF's. However, it is evident that the G_T for outer crack tips *a* and *d* are dominated by mode-I SIF, whereas inner crack tips *b* and *c* are significantly influenced by both modes. Figure 16 also shows that G_T is the largest at crack tip *b* for $0° < \phi(2) < 100°$ and $123° < \phi(2) < 153°$ indicating possible self similar crack propagation within this range. Note that when crack *cd* becomes aligned with the preferred fiber direction, G_T (at crack tip *b*) reaches a minimum while crack tip *c* reaches a maximum. Thus, we may conclude that at this critical configuration, $\phi(2) = 30°$, the inner crack tips *b* and *c* may be driven towards each other and connect to form a macro kinked crack.

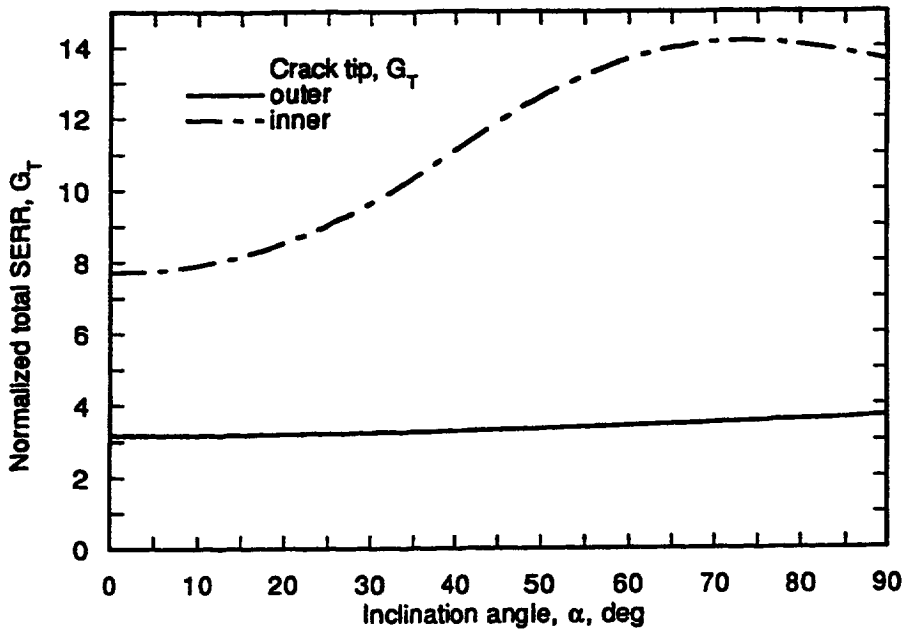

Figure 12: Normalized G_T versus α for two equal noncollinear cracks in a composite plate (strength of anisotropy $E_{LL}/E_{TT} = 40$; reinforced at $\Omega = 45°$; subjected to far-field normal stress, see Fig. 10).

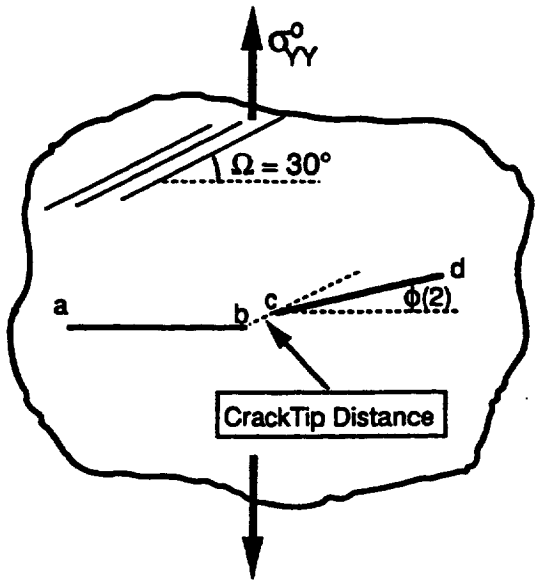

Figure 13: Geometry and loading condition problem of two non-parallel cracks.

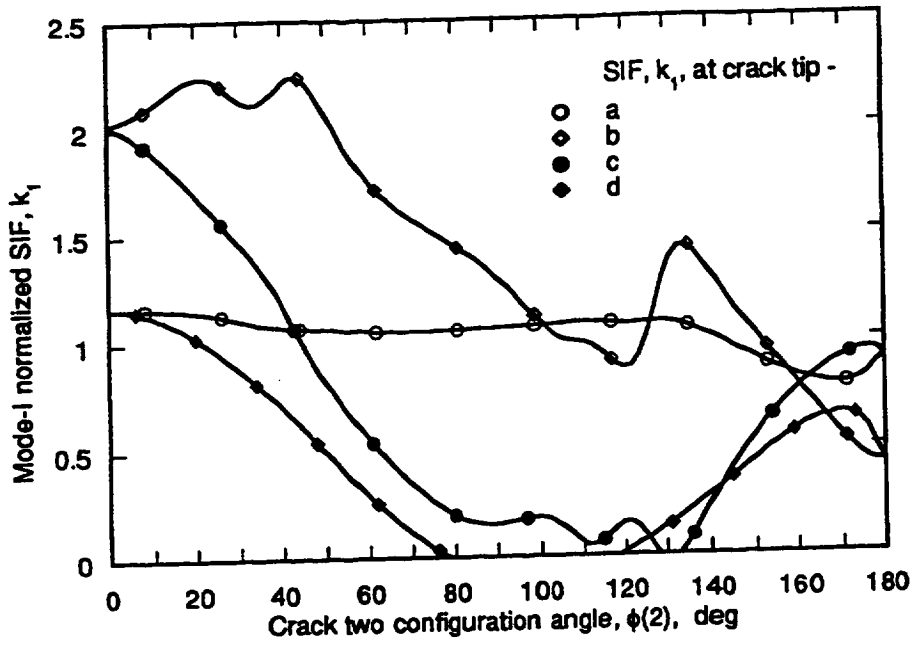

Figure 14: Normalized mode-I SIF's versus crack-2 angle $\phi(2)$ for two equal cracks in a composite plate (strength of anisotropy $E_{LL}/E_{TT} = 40$; reinforced at $\Omega = 30°$; subjected to far-field normal stress, see Fig. 13).

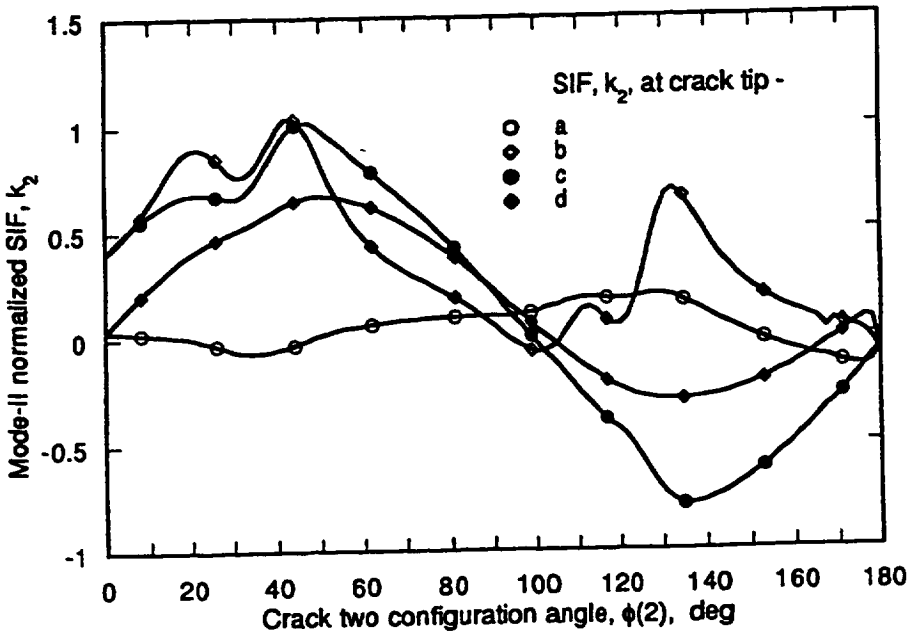

Figure 15: Normalized mode-II SIF's versus crack-2 angle $\phi(2)$ for two equal cracks in a composite plate (strength of anisotropy $E_{LL}/E_{TT} = 40$; reinforced at $\Omega = 30°$;subjected to far-field normal stress, see Fig. 13).

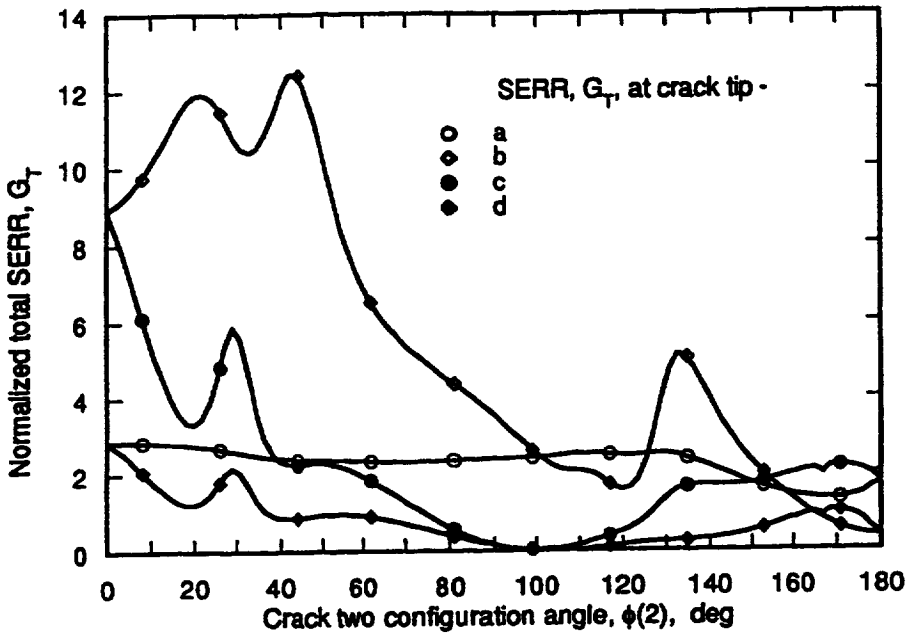

Figure 16: Normalized G_T versus crack-2 angle $\phi(2)$ for two equal cracks in a composite plate (strength of anisotropy $E_{LL}/E_{TT} = 40$; reinforced at $\Omega = 30°$; subjected to far-field normal stress, see Fig 13.

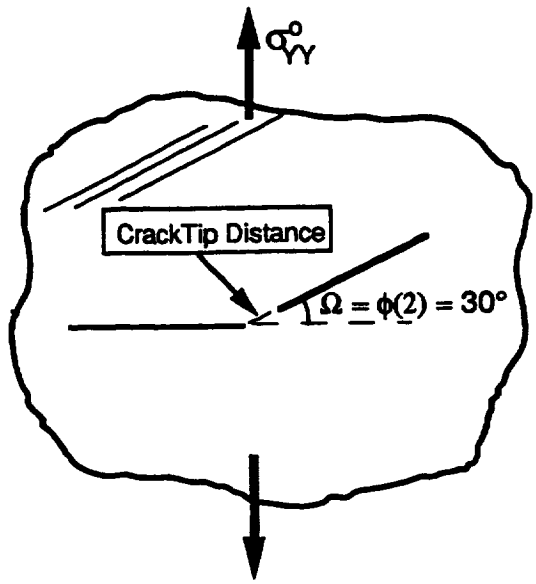

Figure 17: Geometry and loading condition of two inclined cracks.

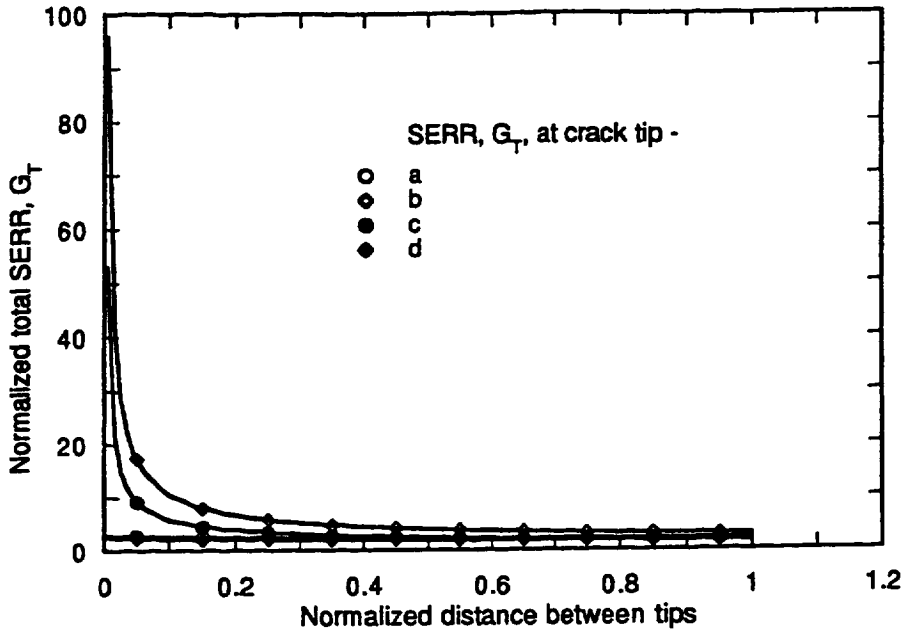

Figure 18: Normalized G_T versus normalized crack tip distance for inclined cracks in a composite plate (strength of anisotropy $E_{LL}/E_{TT} = 40$; reinforced at $\Omega = 30°$; subjected to far-field normal stress, see Fig. 17).

7.1.4 Influence of Crack Spacing

To determine the influence of crack spacing, let us consider the preceding two crack system for the critical configuration $\phi(2) = \Omega = 30°$ and analyze the behavior of these cracks to examine how the G_T varies with respect to the normalized inner crack tip distance d (see Fig. 17). As we would expect, given the results shown in Fig. 13, the G_T's of the outer crack tips are hardly influenced by the change in positions of the cracks. But the G_T's for the inner crack tips (b and c) display a strong interaction, especially for $0 < d < 0.2a_1$, as shown in Fig. 18: the closer the crack tips, the higher the normalized G_T, and thus, the smaller the far-field stress state required to cause the cracks to propagate toward each other.

7.2 Three Crack Interaction

Consider a transversely isotropic plate with a strength of anisotropy $E_{LL}/E_{TT} = 40$ and a three-parallel-crack system as shown in Fig. 19. The two cracks denoted ef and cd are always symmetric, with respect to the horizontal line that coincides with crack ab. First let us keep the distance between inner crack tips b , c, and e (D_h) constant at $0.1a_1$,while the angle Ω , describing the preferred direction, is varied. Mode-I SIF's for tips b, c, and e are shown in Fig. 20. A number of observations can be made from Fig. 20. First, the k_1 for crack tip b resembles an inverted parabola with a maximum at $\Omega = 45°$. Second, k_1 for crack tip b is the largest of the three inner tips - for all preferred directions because of the magnification influence of cracks ef and cd (situated

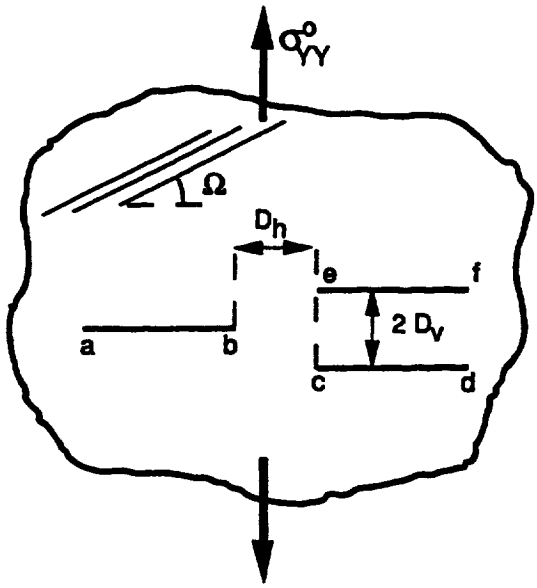

Figure 19: Geometry and loading condition defining three parallel cracks problem.

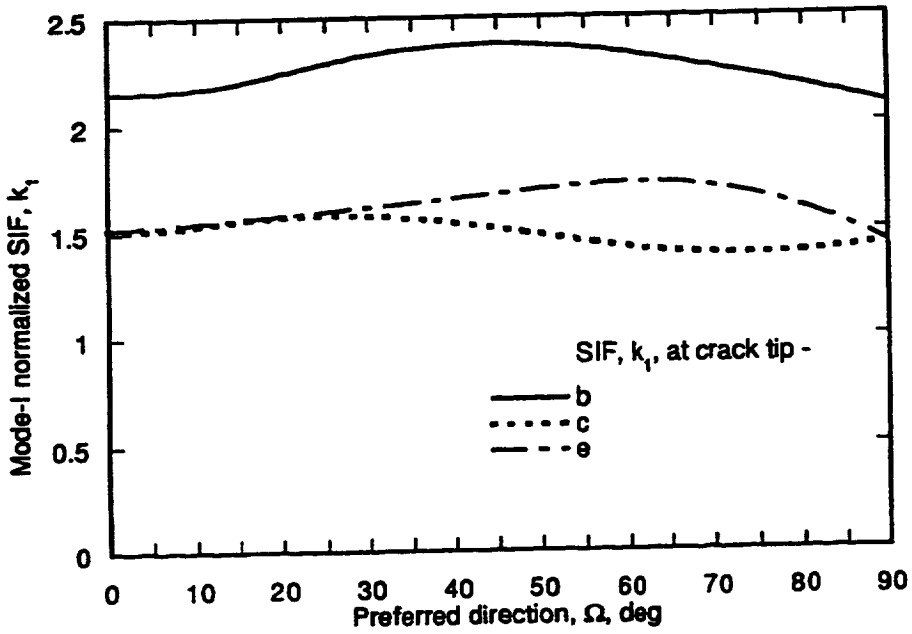

Figure 20: Mode-I normalized SIF's versus Ω for three parallel cracks in a composite plate (strength of anisotropy $E_{LL}/E_{TT} = 40$; subjected to far-field normal stress, see Fig. 19).

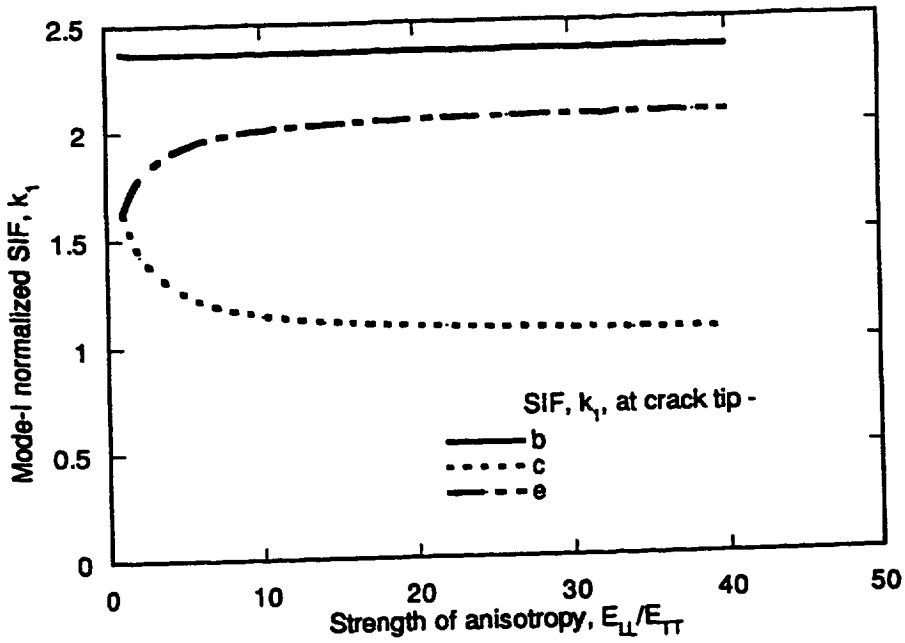

Figure 21: Mode-I normalized SIF's versus strength of anisotropy E_{LL}/E_{TT} for three parallel cracks in a composite plate (reinforced at $\Omega = 60°$; subjected to far-field normal stress, see Fig. 19).

in front of crack ab). Similarly, because of the mutual shielding of the cracks above and below, the k_1 for cracks cd and ef must be smaller . Third, the k_1 at inner tips c and e are identical in the range $0 < \Omega < 25$, but they begin to deviate from one another, in a symmetrical manner, for preferred directions $\Omega > 25°$. Also since k_1 for crack tip e is larger than that for crack tip c, this would suggest that the influence of the singular stresses is transmitted over greater distances along the preferred direction, thus confirming the concept of stress-channeling (or in our case damage channeling) along the preferred direction, as discussed by Spencer[12]. The distance of influence is clearly dependent on the strength of anisotropy specified, as can be seen in Fig. 21.

Mode-II SIF's for the three inner crack tips are shown in Fig. 22. Here, the absolute value of k_2 for crack tip b is approximately zero for the various preferred directions and exactly zero for the orthogonal conditions ($\Omega = 0, 90°$) . The absolute value of k_2 for crack tip e is the largest of the three with a local maximum at $\Omega = 25°$. Again, this is a function of the directional stress channeling effect. Also, note that the absolute values of k_2 for crack tips c and e are identical when the cracks are parallel and normal to the preferred directions; however the magnitude at $\Omega = 0$ is more than twice that for $\Omega = 90$.

The variation of the G_T as a function of preferred direction, for the three inner crack tips b, c, and e are shown in Fig. 23. Clearly, the G_T combines all of the aforementioned characteristics for each crack tip into one convenient parameter that exhibits a strong dependence on the preferred direction angle Ω. Local maxima for these curves are located within a 10° range centered at $\Omega = 45°$. It may be concluded from Fig. 23 that crack propagation is easiest when the preferred direction makes a 45° angle, thus connecting through reinforcement (or damage channeling) crack tips b and e. Hence, as a result of

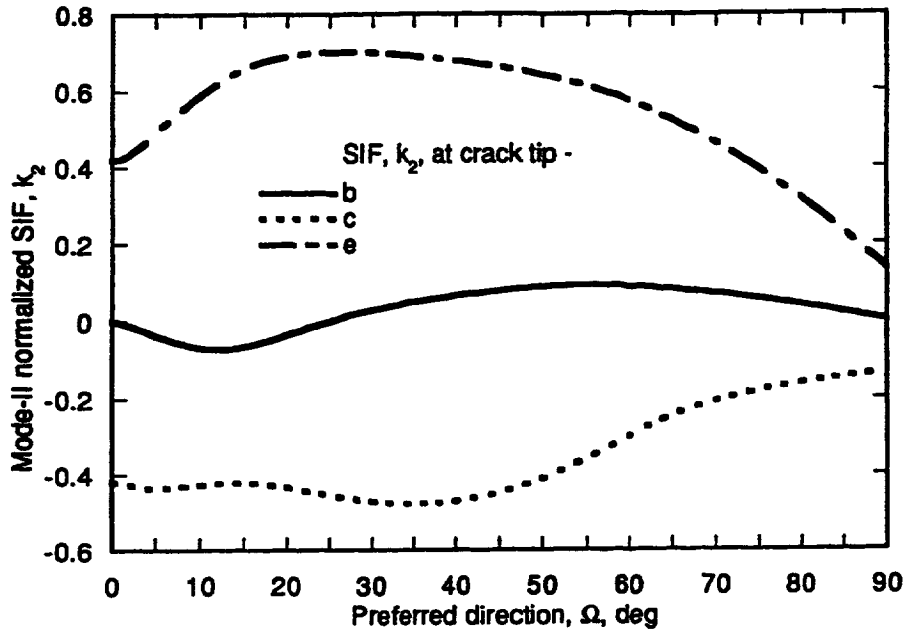

Figure 22: Mode-II normalized SIF's versus angle Ω for three parallel cracks in a composite plate (strength of anisotropy $E_{LL}/E_{TT} = 40$; subjected to far-field normal stress, see Fig. 19).

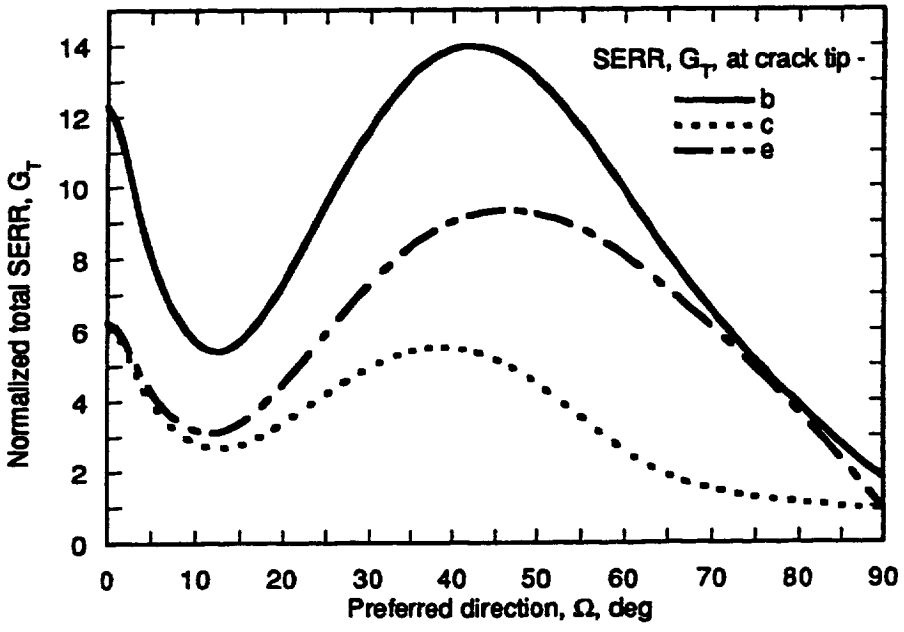

Figure 23: Normalized G_T versus Ω for three parallel cracks in a composite plate (strength of anisotropy $E_{LL}/E_{TT} = 40$; subjected to far-field normal stress, see Fig. 19).

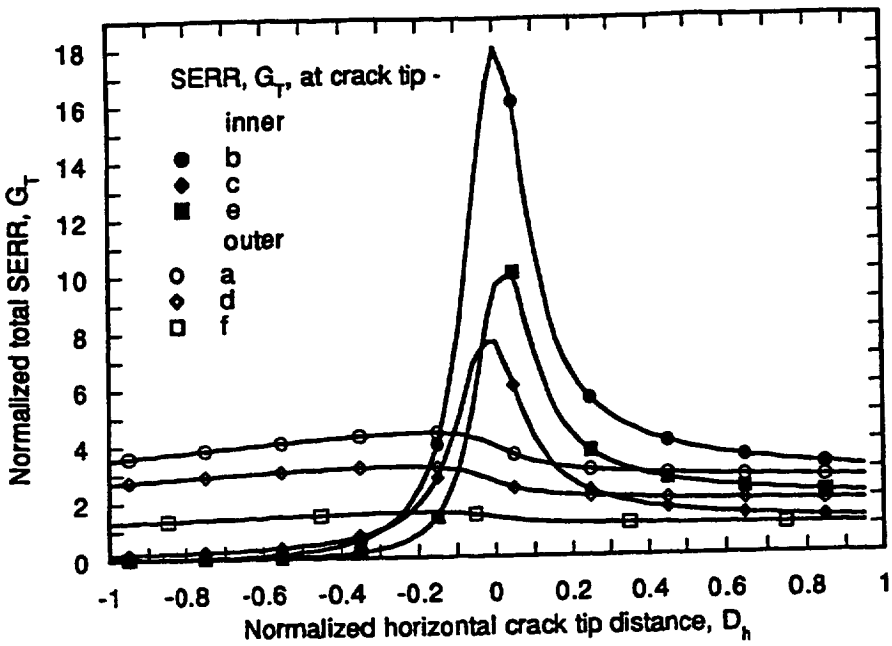

Figure 24: Normalized G_T versus horizontal component of the tip distance D_h for three parallel cracks in a composite plate (strength of anisotropy $E_{LL}/E_{TT} = 40$; reinforced at $\Omega = 45°$; subjected to far-field normal stress, see Fig. 19).

a physical crack propagation, we would anticipate a zigzag crack that develops through the connection of cracks ab and ef .

Last, let us consider the case of two parallel cracks ef and cd that are a fixed vertical distance apart ($D_v = 0.1a_1$) and crack ab is slid in between them. Figure 24 shows the variation of the G_T's for all crack tips as a function of horizontal position D_h for the case when $\Omega = 45°$. When the parameter D_h is zero, tip b is on the same vertical line that connects tips c and e. Thus, when crack ab is away from the parallel cracks $D_h > 0$, and when tip b is between cracks cd and ef , $D_h < 0$. Note that as crack tip b comes closer to the vertical line connecting tips c and e, the G_Ts are magnified; with the amplification factor of the inner crack tips being significantly greater than that of the outer crack tips. Conversely, when $D_h < 0$, all inner tips become strongly shielded, so the inner G_T's sharply drop off, almost to zero. Note that crack tip e has the most rapid decrease and quickly reaches a value less than that of tip c.

7.3 Horizontal Notch Interaction With Three Microcracks

The final problem to be consider in this paper consist of a transversely isotropic plate, with a strength of anisotropy (E_{LL}/E_{TT}) equal to 40, that contains a large horizontal notch (of length $2a_1$) and three radially oriented microcracks (of length $a_2 = a_3 = a_4 = 0.1a_1$), as shown in Fig. 25. The radial distance between the inner tips of the notch and the three microcracks remains fixed at $0.005a_1$, while the orientation (angle Ω) of the preferred direction is varied from 0 to 180°. The G_T's for all the inner microcrack and

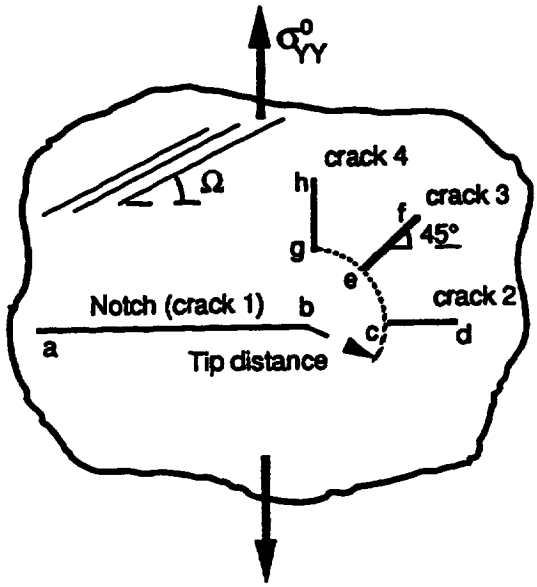

Figure 25: Geometry and loading condition defined for a horizontal notch and three microcrack problem.

notch tips are shown in Fig. 26.

Evidently, the G_T for notch tip b is larger than that for any of the three microcracks except when the orientation is within two small regions: $8° < \Omega < 20°$ and $70° < \Omega < 98°$. At these values the G_T of the inner tip of the 45° microcrack ef becomes greater than that of the notch. All G_T curves display strong and complex dependence on the orientation. Numerous local extrema exist with the maxima being noted as follows: for notch tip b, the local maxima occur at 0, 38, and 140°; for microcrack tip g, a maximum occurs at 30°; for microcrack tip e, maxima occur at 15, 80, and 155°; and for the horizontal microcrack tip c, the maxima occur at 0°, 40°, and 150°. Again, if the maximum-G_T criterion is used to predict crack propagation, we may conclude that the crack will kink by connecting with crack ef for the preferred direction when $8° < \Omega < 20°$ and $70° < \Omega < 98°$; otherwise it will propagate in a self-similar manner.

Now let us orient the preferred direction Ω at a fixed angle of 15° and vary the radial inner tip distance between notch tip b and the three microcrack tips c, e, and g. Figure 27 shows the amplification effect (which becomes noticeable when the tip distance is less then $0.1a_1$) resulting from the complex interaction of the cloud of microcracks with the larger notch crack. Clearly, the G_T for notch tip b is the largest until the tip distance is decreased to approximately $0.04a_1$, whereupon the G_T for the microcrack inclined at 45° drastically increases — exceeding all other curves and creating the condition for the crack to kink.

Finally, let us discuss the influence of the strength of anisotropy, as shown in Fig. 28. Here, we assume that the preferred direction and radial tip distance are held constant at $\Omega = 15°$ and $0.005a_1$, respectively, while the strength of anisotropy E_{LL}/E_{TT} is varied. When the material is isotropic (i.e., $E_{LL}/E_{TT} = 1$) the G_T at notch tip b far surpasses

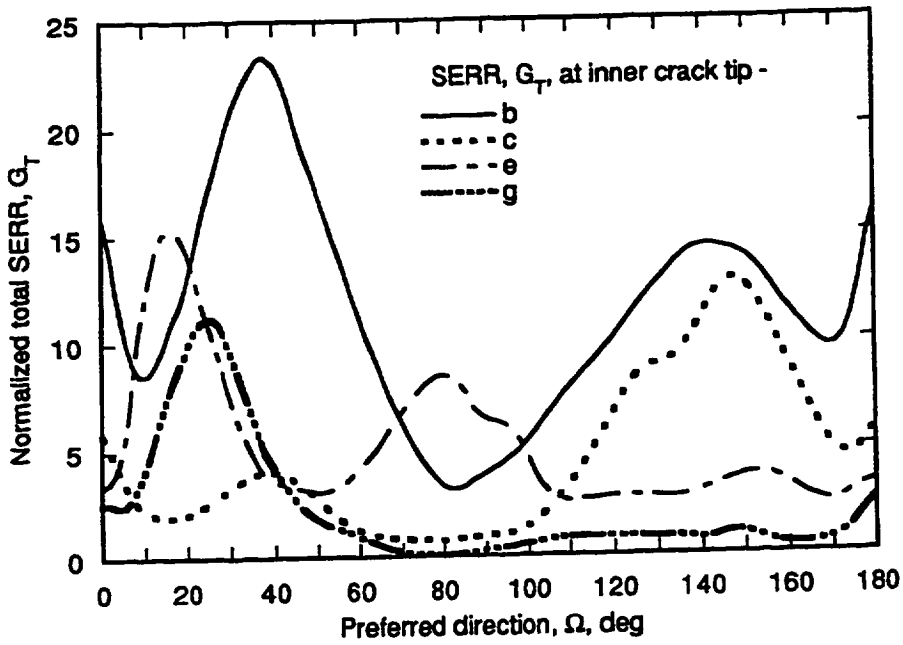

Figure 26: Normalized G_T versus Ω for notch and three microcrack inner tips in a composite plate (strength of anisotropy $E_{LL}/E_{TT} = 40$; tip distance, $0.005a_1$; subjected to far-field normal stress, see Fig. 25).

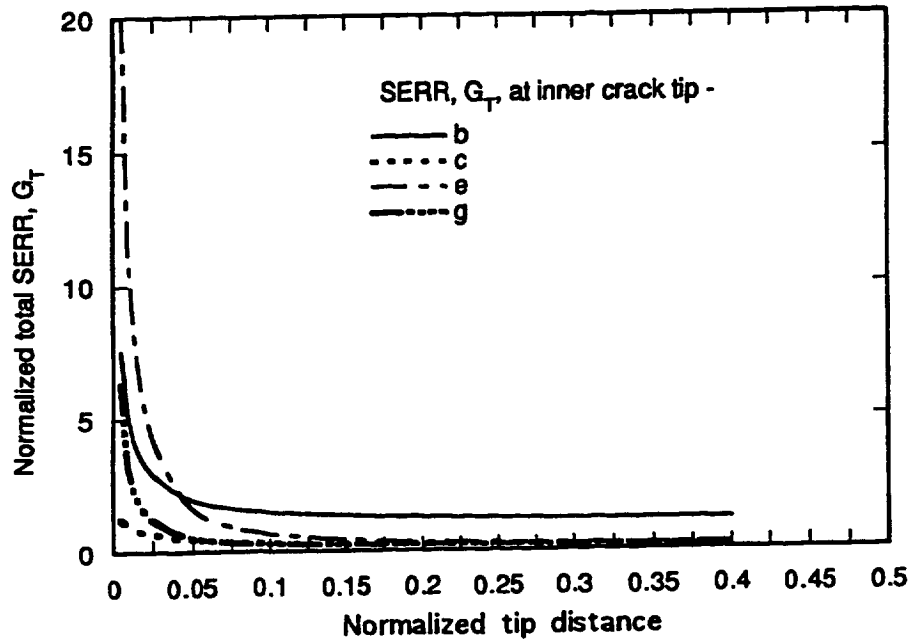

Figure 27: Normalized G_T versus normalized tip distance between inner tips of notch and three microcrack in a composite plate (strength of anisotropy $E_{LL}/E_{TT} = 40$; reinforced at $\Omega = 15°$; subjected to far-field normal stress, see Fig. 25).

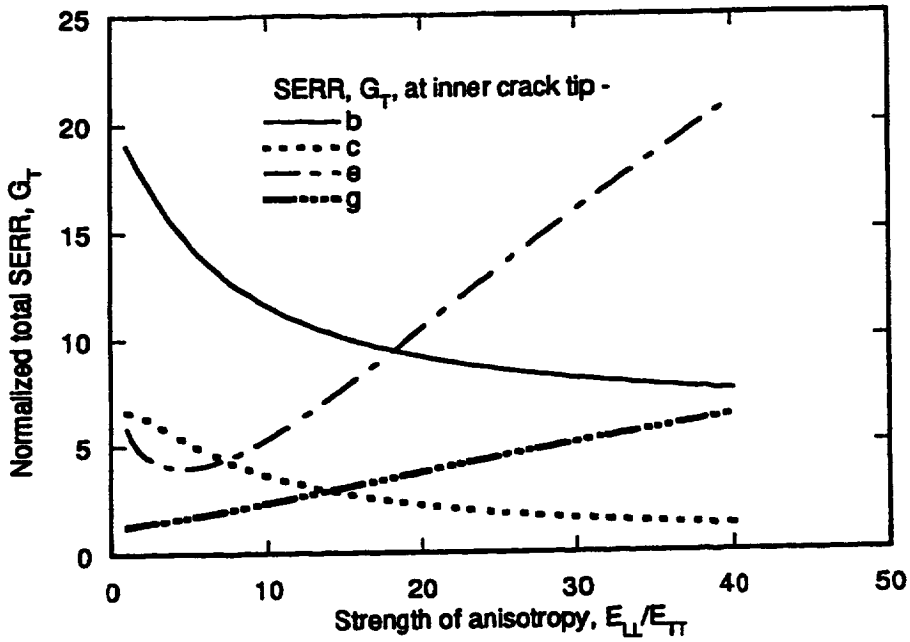

Figure 28: Normalized G_T versus strength of anisotropy E_{LL}/E_{TT} for inner tips of notch and three microcracks in a composite plate (reinforced at $\Omega = 15°$, tip distance, $0.005a_1$; subjected to far-field normal stress, see Fig. 25).

the G_T's of the remaining microcrack inner tips. However, even a small change in the strength of anisotropy significantly influences the value of the G_T for all inner crack tips. Note that when $E_{LL}/E_{TT} > 18$, the G_T for the inclined microcrack tip e becomes the largest. And since the crack having the highest G_T will propagate first, a kinked crack will be generated by connection of crack ef to notch ab.

8 CONCLUDING REMARKS

A rigorous formulation has been presented for calculating the crack-opening displacement, SIF and G_T at the various crack tips of a multicracked anisotropic medium. This formulation has been shown to simplify exactly to our previous isotropic formulation which was validated for a number of published crack orientations. The size, orientation, and distribution of all cracks were considered to be independent parameters of the solution. This unique formulations is computationally efficient and offers accurate solution capability. It allows us to easily perform numerous parametric studies to analyze the contribution of each parameter on the local stress field and the characteristics of the damage progression in an anisotropic (e.g., transversely isotropic) material.

The problems of two and three, collinear and non-collinear, interacting cracks were examined. By varying the strengths of anisotropy, we showed that materials with preferred off-axis directions relative to the applied load produced highly mixed-mode crack propagation, even when only mode-I type crack geometry was present. A small change in the strength of anisotropy (when $0 < E_{LL}/E_{TT} < 5$) was shown to highly influence

the G_T and crack-opening displacements for a given tip. These parameters then reached a plateau when $E_{LL}/E_{TT} > 15$. Consequently, even slightly anisotropic materials should be analyzed by using the fully anisotropic approach discussed in this paper.

Modified stiffness parameters (MSP's) were presented as a function of strength of anisotropy and preferred direction. We concluded that $E^{(1)}_{xy}$ and $E^{(2)}_{yy}$ are proportional to the square root of the effective Young's module in the local $x-$ and y-direction, respectively, and that the other two MSP's are identical (i.e., $E^{(2)}_{xy} = E^{(1)}_{yy}$) and related to b_{16} and b_{26} such that they vanish under orthotropic and isotropic conditions.

The discrete auxiliary functions were shown to be related to the crack-opening displacements Δu and Δv. We showed that for cases in which the preferred direction and the applied stress do not coincide (i.e., off-axis orientations), a mode-I local stress field is produced under **mixed-mode** local deformations, or alternatively, mode-I normal deformation results in a **mixed-mode** local stress field. Furthermore, the total G_T was shown to be the most complete anisotropic fracture parameter (because of its sensitivity in detecting changes in the strength of anisotropy and preferred direction). Thus we suggest that for an anisotropic material it should be used as the crack propagation criterion instead of the SIF.

Interaction effects were demonstrated for all fracture parameters. Amplification of the G_T and/or the SIF was shown to occur when cracks were located in front of the main crack. Conversely, reductions in the G_T or SIF were observed when shielding of a crack, by other cracks located above and/or below it, was present. Finally, stress or damage channeling was discovered to play a significant role in the mechanisms that govern crack interaction, in that, stresses were channeled along the preferred direction, causing nonsymmetric interaction, even in the presence of symmetric crack configurations.

References

[1] Timoshenko, S.; Goodier, I.N. (1969):**Theory of Elasticity**. Third ed., McGraw Hill, New York.

[2] Binienda, W.K.; Arnold, S.M.; Tan, H.Q.; and Xu, M.H. (1993): Stress Intensity Factors in a Fully Interacting, Multicracked, Isotropic Plate. Comp. Mech., Vol. 12, no. 5, pp. 297-314.

[3] Erdogan F. (1978) Mixed Boundary-Value Problems in Mechanics. Mechanics Today, S. Nemat-Nasser ed., Vol. 4, Pergamon Press, New York, pp. 1-32.

[4] Badaliance R.; Gupta,G. G. (1976): Growth Characteristics of Two Interacting Cracks. Eng. Fract. Mech., Vol. 8, no. 2, pp. 341-353.

[5] Delale, F.; Erdogan,F. (1977): The Problem of Internal and Edge Cracks in an Orthotropic Strip., J. Appl. Mech., Vol. 44, no. 6, pp. 237-242.

[6] Delale, F.; Erdogan, F. (1979): Bonded Orthotropic Strips with Cracks. Int. J. Fract., Vol. 15, no. 8, pp. 343-364.

[7] Delale, F.; Bakirtas,I; Erdogan, F. (1979): The Problem of an Inclined Crack in an Orthotropic Strip., J. Appl. Mech., Vol. 46, no.3, pp. 90-96.

[8] Cherepanov G.P., "Mechanics of Brittle Fracture", McGraw-Hill, N.Y. 1979.

[9] Horii, H.; Nemat-Nasser, S. (1985): Elastic Fields of Interacting Inhomogeneities. Int. J. Solids Struct., Vol. 21, no. 7, pp. 731-745.

[10] Agarwal, B.D., and Broutman, L.J.(1980): **Analysis and Performance of Fiber Composites**, John Wiley & Sons, Inc.

[11] Erdogan F. (1962): On The Stress Distribution in Plates with Collinear Cuts Under Arbitrary Loads. Proceedings of the Fourth U.S. National Congress of Applied Mechanics, Vol. 1,ASME, New York, pp. 547-553.

[12] Spencer, A.J.M. (1972): **Deformations of Fibre-reinforced Materials**, Clarendon Press, Oxford.

REPORT DOCUMENTATION PAGE

Form Approved
OMB No. 0704-0188

Public reporting burden for this collection of information is estimated to average 1 hour per response, including the time for reviewing instructions, searching existing data sources, gathering and maintaining the data needed, and completing and reviewing the collection of information. Send comments regarding this burden estimate or any other aspect of this collection of information, including suggestions for reducing this burden, to Washington Headquarters Services, Directorate for Information Operations and Reports, 1215 Jefferson Davis Highway, Suite 1204, Arlington, VA 22202-4302, and to the Office of Management and Budget, Paperwork Reduction Project (0704-0188), Washington, DC 20503.

1. AGENCY USE ONLY (*Leave blank*)	2. REPORT DATE	3. REPORT TYPE AND DATES COVERED
	January 1995	Technical Memorandum

4. TITLE AND SUBTITLE
Driving Force Analysis in an Infinite Anisotropic Plate With Multiple Crack Interactions

5. FUNDING NUMBERS
WU-505-63-12
NAG3-1223

6. AUTHOR(S)
Wieslaw K. Binienda and Steven M. Arnold

7. PERFORMING ORGANIZATION NAME(S) AND ADDRESS(ES)
National Aeronautics and Space Administration
Lewis Research Center
Cleveland, Ohio 44135-3191

8. PERFORMING ORGANIZATION REPORT NUMBER
E-9401

9. SPONSORING/MONITORING AGENCY NAME(S) AND ADDRESS(ES)
National Aeronautics and Space Administration
Washington, D.C. 20546-0001

10. SPONSORING/MONITORING AGENCY REPORT NUMBER
NASA TM-106838

11. SUPPLEMENTARY NOTES
Wieslaw K. Binienda, The University of Akron, Akron, Ohio 44325-3905 (work funded by NASA Grant NAG3- 1223). Responsible person, Steven M. Arnold, organization code 5220, (216) 433-3334.

12a. DISTRIBUTION/AVAILABILITY STATEMENT
Unclassified - Unlimited
Subject Category 24

This publication is available from the NASA Center for Aerospace Information, (301) 621-0390.

12b. DISTRIBUTION CODE

13. ABSTRACT (*Maximum 200 words*)

The methodology and a rigorous solution formulation are presented for stress intensity factors (SIF's, k) and total strain energy release rates (SERR, G_T) of a multicracked plate, that has fully interacting cracks and is subjected to a far-field arbitrary stress state. The fundamental perturbation problem is derived, and the steps needed to formulate the system of singular integral equations whose solution gives rise to the evaluation of the SIF's are identified. Parametric studies are conducted for two, three and four crack problems. The sensitivity and characteristics of the model is demonstrated.

14. SUBJECT TERMS	15. NUMBER OF PAGES
Fracture mechanics; Anisotropy; Multiple cracks; Elastic	40
	16. PRICE CODE: A03

17. SECURITY CLASSIFICATION OF REPORT	18. SECURITY CLASSIFICATION OF THIS PAGE	19. SECURITY CLASSIFICATION OF ABSTRACT	20. LIMITATION OF ABSTRACT
Unclassified	Unclassified	Unclassified	